ACUSTICA · acta acustica
Vol 84 (1998) 543 – 562

Mechanics of the Contact Area Between a Violin Bow and a String. Part I: Reflection and Transmission Behaviour

R. Pitteroff and J. Woodhouse*
Cambridge University Engineering Department. Trumpington St, Cambridge CB2 1PZ, U.K.

Summary
A detailed physical model of behaviour in the contact area between a violin bow and a string is developed and explored. The model takes into account the finite width of the bow, the bending stiffness of the string, the longitudinal bow-hair compliance and the torsional motion of the string. It is designed for implementation in an enhanced numerical simulation of the bowed-string action, the topic of two companion papers [1, 2]. This paper describes an analytical investigation of the wave reflection and transmission behaviour, when a wave on the string is incident on the bow. The predictions are compared with experimental results by Cremer [3], Lazarus and Eisenberg [4]. Comparison shows that longitudinal bow-hair compliance has a large impact on the reflection and transmission behaviour and that sensible modelling of the finite width of the bow requires modelling of the bow-hair compliance. In general, bending stiffness plays a minor role.

PACS no. 43.75.De, 43.40.Cw

1. Introduction

Most models of the action of the bowed string assume a point contact between bow and string, but every player of a bowed instrument is aware that the sound quality and the bow handling may be varied by altering the amount of bow-hair one brings into contact with the string (by tilting the bow). To date very little research into the effect of the width of the bow on the string vibration has been published. Raman [5] investigated the implications of finite bow width for his dynamical model and states "while it is possible for a single point on the string to have absolutely the same velocity as the bow in every part of its forward motion, kinematical theory shows that it is not possible for every element on a finite region to have absolutely the same velocity as the bow in every part of its forward motion."

In his model Raman allowed neither for torsional motion, in other words for the string to twist and roll against the bow, nor for longitudinal deformation of the bow-hair. He therefore had to conclude that even during the sticking phase of the Helmholtz cycle the string would be sticking to the bow permanently only at one point while the remainder of the string in the bowed region would be slipping relative to the bow-hair.

Friedlander [6] suggested that "to the first order, the effect of the finite width of the bow can be allowed for by assuming that the portion of the string in contact with the bow moves as a rigid body, and can be replaced by a particle ... attached to the string at the bowing point". He discussed briefly what this would imply for the possible regimes of vibration. He deduced from his analysis that the additional inertia term makes continuous motion more likely than discontinuous motion and that it would affect the period length. His analysis will be discussed below. His model remains a point-bow model despite this adjustment and cannot provide a satisfactory answer to the question raised by Raman.

The most extensive study of the possible effects of the width of the bow has been presented by McIntyre *et al.* [7, 8]. The authors explain that, particularly when bowing close to the bridge, the string may occasionally slip at one side of the bow (usually the one closer to the bridge) while continuing to stick at the other side. The cause of these "differential-slipping" events is precisely the incompatibility of ideal Helmholtz motion and the uniform bow velocity across the width of the bow which was pointed out by Raman. Simulation runs with a two-bowing-point, "rounded-corner model" confirmed this explanation: good qualitative agreement was obtained with waveforms obtained by bowing with a "bow" having just two points of contact, and these in turn were in qualitative agreement with results obtained with a normal bow. These differential-slipping events are of importance in instrument playing because they generate irregular spikes in the "bridge force", the transverse force exerted by the string at the bridge, which result in audible noise.

To construct a model of a bow of finite width which goes beyond this two-point model, several other physical effects need to be taken into account. The first of these is the bending stiffness of the string. The evanescent fields arising from bending stiffness are likely to have a comparable length-scale to that of the bow width and must be allowed for. The effect of dispersive wave propagation between bow and string terminations due to bending stiffness has been studied by Woodhouse [9]. The effect of bending stiffness in the vicinity of the contact of bow and string, however, has received little attention. Cremer [3] attributes the frequency-dependent reflection and transmission behaviour for waves impinging on the bow to bending stiffness ([3] page 146), but on the other hand holds the view that string damping must round off the shape of the string to such an extent that bending stiffness no longer plays a role ([3] page 152). Boutillon [10] incorporates bending stiffness into an analytical calculation of the playing frequency for a given waveform.

The next physical effect to be considered is longitudi-

Received 17 June 1996,
accepted 17 September 1997.

* To whom correspondence should be sent

ACUSTICA · acta acustica
Vol. 84 (1998)

nal bow-hair compliance. The effects of longitudinal bow-hair compliance have been discussed qualitatively by Schumacher [11] and Cremer [3]. Schumacher argues that bow-hair compliance may allow the velocity of the bow-hair at the point of contact to differ from the nominal bow velocity by up to 12%. Cremer dismisses the possibility of non-negligible effects due to bow-hair compliance; he argues that the ratio of bow-hair impedance to string impedance is too high for such effects to be important. Adrien and Ducasse [12] have presented a point-bow model taking into account bow-hair compliance but no thorough physical investigation seems to have been conducted. More recently bow-hair compliance has been implemented into a model of point-bow excitation of an ideal flexible string by Guettler [13]. He reports that due to losses in the model bow, computed simulations can achieve shorter initial transients.

The final physical effect to consider is string torsion. It is widely recognised that torsional motion occurs on real bowed strings and the more elaborate investigations using point-bow models take this into account. In the context of the finite-width bow, torsional motion plays an important role in bridging the incompatibility of the Helmholtz motion and the uniform bow velocity across the width of the bow. In any case, torsion should be included in any realistic bowed-string model because strings used on instruments exhibit much higher rates of torsional damping than transverse damping [14]. The transverse waves are more relevant in terms of sound production but a fraction of the energy carried by transverse waves is converted into torsional wave energy when transverse waves impinge on the bow. This converted wave energy is then subject to the higher rate of torsional damping. Because of reciprocity the rate of energy conversion for torsional waves impinging on the bow is of course the same. However, torsional waves departing from the bow will have lost a considerable amount of their energy during their journey to the terminations of the string and back. Hence, the transverse motion is damped. It has been suggested by McIntyre *et al.* [7] that the undesirable subharmonics excited during initial transients lose their energy through this mechanism of energy conversion and dissipation. It will emerge that the rate of energy conversion itself is a function of frequency and is affected by bending stiffness, bow-hair compliance and the bow width.

The point of departure for the present investigation is a scattering experiment that Cremer [3], Lazarus and Eisenberg [4] developed to provide some insight into the mechanics of the contact area of bow and string. A stationary bow was placed on a very long string and a bow force sufficiently high to prevent slipping was applied. ("Bow force" is the normal force between bow-hair and string, denoted F_b.) Transverse wave packets were generated on the free string, in the plane of string and bow-hair, and travelled to meet and interact with the bow. Incident, reflected and transmitted waves were monitored to establish the frequency dependence of the reflection and transmission coefficients. Some of the experimental results obtained by Eisenberg and Lazarus [4] have not been explained satisfactorily to date. The experiment was designed to study the regime in which the string sticks to the bow throughout, with no slipping. This problem of a string sticking to a bow and rolling can be treated as a linear problem, which lends itself to an analytical approach. Cremer's [3] theoretical model of this system assuming a rigid point bow on a stiff string led him to the conclusion that bending stiffness is responsible for the observed frequency dependence of the reflection and transmission coefficients.

This work takes Cremer's modelling approach further by introducing the finite bow width and by modelling the longitudinal bow-hair compliance. In Section 2 the behaviour of bow-hair is studied. In Section 3 a theoretical model for the contact area of string and bow is developed starting from Cremer's simple case. Predictions of this new model, which takes the finite bow width and the longitudinal bow-hair compliance into account, are compared with the results from the experiment described above. Evidence will be presented that Cremer's interpretation of the experimental results is rather misleading. Bending stiffness is by no means the dominant effect in the present model: longitudinal bow-hair compliance produces much stronger effects. Incorporating finite width into Cremer's *rigid* point-bow model — a potential improvement — reveals that the assumption of a rigid bow necessarily leads to non-physical results, namely singular (delta-function type) friction forces at the edges of the bow. An infinite value of the frictional coefficient would be necessary for sticking to be possible at the edges. Finite longitudinal bow-hair compliance will be shown to alleviate this problem. The non-physical singular forces are spread out into finite regions near the edges of the bow, so that sticking over the whole bow width is possible.

This investigation of the contact area without the complications added by the nonlinear process of bowing enables us to determine which physical properties of string and bow are most likely to be important in a full-fledged simulation model of the bowed string. Such a simulation model is developed and explored in two companion papers [1, 2], referred to herein as Part II and Part III. Although we will usually speak of the violin, this investigation pertains to all instruments of the violin family.

2. Bow-hair

2.1. Material properties

The surface structure and histology of bow-hair have been treated in a few publications [15, 16] but very little seems to be known about its mechanical properties. Any investigation of the material behaviour is hampered by the fact that bow-hair is inhomogeneous: properties may vary from hair to hair within a bundle taken from the same horse, and along the length of an individual hair the diameter and material properties vary from the fresh growth at the base to the older hair at the tip.

Three types of simple experiment designed to measure the value of the complex Young's modulus were carried out. First, the real part E_H of the Young's modulus was measured in a standard quasi-static tensile test. The stress-strain

relation was found to be linear for a large range in stress, a range greatly in excess of what is encountered in actual bowing. Values of $E_H = 7 \pm 0.5$ GPa were found. A breaking strain of 0.2 was observed. Elastic and plastic deformation accounted for approximately 30% and 70% of the breaking strain respectively.

A second estimate of E_H can be derived from the phase velocity c_H of longitudinal waves on the hair and the mass density ρ_H, as was done by Schumacher [11, 17]. He determined c_H on single hairs by measuring the time of flight of impulses and by recording the normal modes for frequencies up to 10 kHz, and found $c_H = 2500$ m/s ± 3 % [18]. According to our measurements the mass density is $\rho_H \approx 1100$ kg/m^3. The resulting value for the Young's modulus is $E_H = c_H^2 \rho_H \approx 7$ GPa. The mass density was determined by measuring the volume of an accurately weighed bundle of hair. This was done by submerging the hair in a volumetric flask filled with water and weighing the flask content. Air bubbles caught in the hair were removed with the help of ultrasound.

The third approach used vibrational tests. A mass incorporating an accelerometer was suspended by a single hair, hanging vertically, and impulsively excited. The resulting frequency and decay rate give information about the real and imaginary parts of the Young's modulus under dynamic loading. The hair length was varied between 0.03 m and 0.6 m and the mass between 11 g and 62 g, which produces a frequency range of roughly 10–100 Hz. These tests were performed on the "fresh" and the "old" parts of a hair and, finally, on the entire hair. The measurements demonstrate that the assumption of a lightly damped oscillator with exponential time-decay in amplitude $e^{-\delta t}$ is justified. Aerodynamic damping is negligible. If the length of hair is thought of as a massless spring, the spring constant and hence the real part of the Young's modulus is readily derived from the mass, the eigenfrequency and the hair diameter. The hair diameters used in the data analysis were obtained by averaging the diameter over the length of the "old" and the "fresh" halves of the hair individually. Values of $E_H = 9 \pm 1.5$ GPa are found. There is a definite trend with frequency (see Figure 1), with the higher values of E_H lying in the lower part of the frequency range investigated.

For the longer samples, which also correspond to the lower third of this frequency range, the values are a little higher than those from the static tests, possibly because of the influence of creep in the latter. At higher frequencies, the value of E_H is not inconsistent with that derived from the longitudinal wave velocity. It appears that "old" growth is less elastic than "fresh" growth. Correcting for the clamped end of the hair has very little effect. Uncertainty regarding the hair diameter ($\pm 5\%$) and errors in the measurement of the eigenfrequency ($\pm 2.5\%$) can affect these results significantly ($\pm 15\%$).

The rate of exponential decay δ of the oscillation was found to be dependent on the eigenfrequency of the system and on the length of the hair, varying from 1 s^{-1} to 14 s^{-1} (Figure 2(a)). For a sample of given length higher frequencies are associated with higher decay rates. "Fresh" hair consistently showed a smaller decay rate than "old" hair

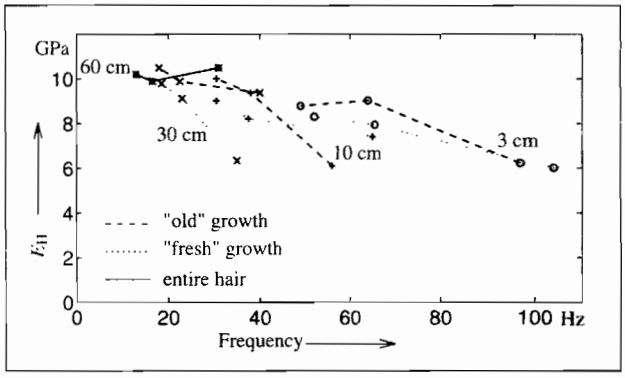

Figure 1. The real part E_H of the Young's modulus of bow-hair derived from the eigenfrequency, the mass and the hair diameter of one-hair oscillators. The lines connect data points obtained from the same sample of a given length with different attached masses.

(10–30%). The amplitude of the excitation impulse had little effect ($\pm 5\%$). If the oscillator is seen as a mass M suspended from a lumped spring S and a lumped dashpot D in parallel, one can identify a damping constant $D = 2M\delta$, shown in Figure 2(b). In general short samples exhibit higher damping constants than long samples.

In terms of a complex Young's modulus $E_H(1 + i\xi_H)$, the results indicate that the loss factor $\xi_H = 2\delta/\omega_0$, where ω_0 is the radian eigenfrequency of the system, is not independent of frequency even in this small low-frequency range. Values of the order of $\xi_H = 0.02$–0.05 were found (Figure 2(c)). All samples, especially the longer ones which are most relevant for the modelling of the bow, show a significant increase in loss factor with frequency.

2.2. Modelling the bow-hair

In this section constitutive equations are developed for the longitudinal compliance of bow-hair. The ribbon of bow-hair of a violin bow consists of approximately 200 hairs of which no more than 50 are in immediate contact with the string. The diameter of an individual bow-hair (0.16–0.25 mm) and the typical distance between adjacent hairs are both small compared to the wavelengths of string vibration one wishes to resolve. Following this argument the ribbon of bow-hair is modelled as a homogeneous continuum and not as a number of discrete hairs.

Furthermore, it will be assumed that only one layer of bow-hair is involved in the bowing process as too little is known about the interaction of the hairs in contact with the string with the rest of the hairs. Presumably the degree to which the friction force affects other layers decreases with their distance from the string as relative motion between layers is likely to occur. Such effects may well depend on the value of the (normal) bow force. Experiments using a mono-layer bow — one layer was separated from the rest of the hair with the help of small wedges — to bow a violin by a bowing machine capable of executing repeatable bow strokes seem to justify the mono-layer model: at moderate bow-force levels bowing with the mono-layer bow produces

ACUSTICA · acta acustica
Vol. 84 (1998)

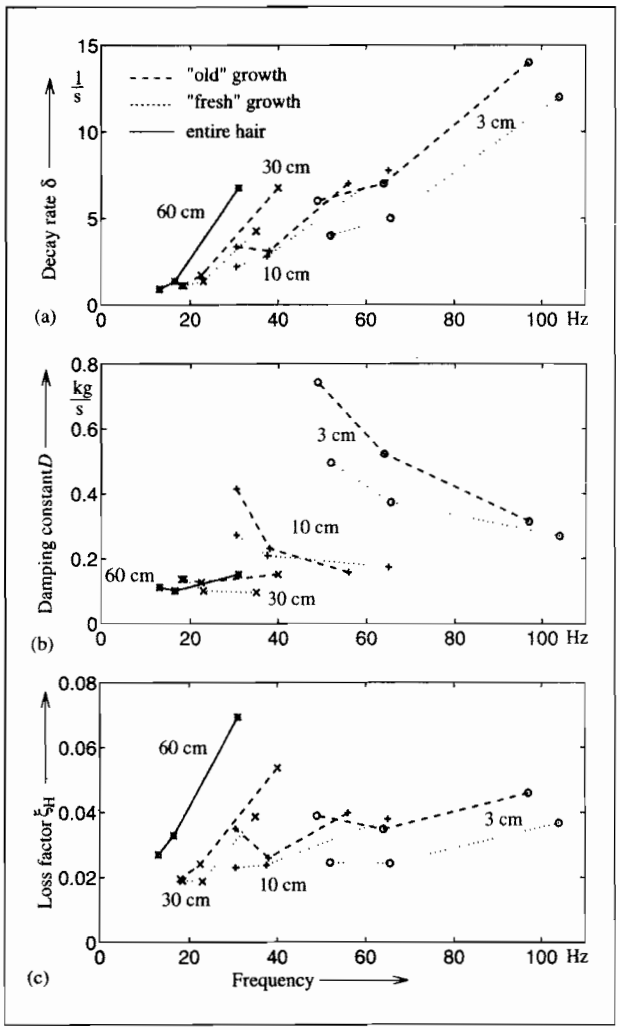

Figure 2. Experimental results on bow-hair damping from mass-spring oscillators. (a) Rates of exponential decay δ versus frequency. (b) Damping constants D and (c) loss factors ξ_H computed from the decay rates. The lines connect data points obtained from the same sample of a given length with different attached masses.

radiated sound which is virtually indistinguishable from that produced using a bow with full hair.

At present little is known about the behaviour of the ribbon of bow-hair mounted on the bow-stick. As was pointed out by Schumacher [11], the longitudinal compliance of the entire ribbon of bow-hair is strongly influenced by the vibrational behaviour of the bow-stick. To allow for this would complicate the model considerably. However, a useful simplifying assumption can be made. In an investigation of the specific effects of finite bow width the concern is mainly with the effect of *differential motion* of the hairs within the contact region, since this is the mechanism by which the singular edge forces mentioned above are removed. The dynamics of the bow stick can only influence differential motion of the hair if the two ends (tip and frog) rotate relative to one another in the bowing plane, and this is probably a small effect. As a first approximation, we ignore it.

We can now model the linear vibrational behaviour of the bow-hair. Two simple approaches were tried: each "filament" of hair can be approximated either by a massless spring acting in parallel with a dashpot, or, more realistically, by a viscoelastic continuum rigidly terminated at the two ends of the bow.

The first approach, the "spring-dashpot" model, leads directly to a constitutive relation

$$f(x,t) = -\left(s\,\eta_H(x,t) + d\,\frac{\partial \eta_H(x,t)}{\partial t}\right), \qquad (1)$$

where f is the force acting on the bow-hair in the longitudinal direction, η_H the bow-hair displacement relative to the (rigid) bow-stick, s the spring constant and d the damping constant. (The distributed quantities f, s and d are all defined per unit length across the width of the ribbon of bow-hair.) The x-axis is in the direction of the string (see Figure 4). For time-harmonic excitation $e^{i\omega t}$, we may write

$$f = -z_H\,\frac{\partial \eta_H}{\partial t}, \qquad (2)$$

with the distributed input impedance of the bow-hair

$$z_H = -\frac{is}{\omega} + d. \qquad (3)$$

For the second approach, the frequency response of a finite viscoelastic continuum terminated rigidly at both ends is easily derived. If the excitation is assumed to be at $\gamma\, l_H$ where γ denotes the relative distance of the excitation point from the frog and l_H the length of the hair, the distributed input impedance is

$$z_H = \frac{i z_\infty}{2\sqrt{1+i\xi_H}}\,\frac{\sin k_H\, l_H}{\sin k_H\,\gamma\, l_H\ \sin k_H\,(1-\gamma)\, l_H} \qquad (4)$$

where z_∞ is the distributed input impedance of the infinite loss-free transmission line and k_H and c_H are the wavenumber and phase velocity for longitudinal waves on the hair. If a number n_H of hairs of length l_H and radius a_H constitute a mono-layer ribbon of width b then:

$$z_\infty = 2\,c_H\,m_H, \quad k_H = \frac{\omega}{c_H}\,\frac{1}{\sqrt{1+i\xi_H}}, \qquad (5)$$

$$c_H = \sqrt{\frac{E_H}{\rho_H}}, \quad m_H = \frac{\rho_H\, n_H\, \pi\, a_H^2}{b}. \qquad (6)$$

Further assumptions concerning the dimensions of the ribbon of bow-hair are necessary to provide numerical values of the constants when implementing the two models in computations. The model violin-bow is a mono-layer of nominal width $b = 10$ mm made up of $n_H = 50$ hairs of diameter $2a = 0.19$ mm and length $l_H = 0.65$ m. It is assumed that the real part of the Young's modulus is $E_H = 7$ GPa, the value found for higher frequencies according to Figure 1 and in static tests, the mass density $\rho_H = 1100$ kg/m^3 and that the force is applied at mid-point lengthwise ($\gamma = 0.5$). The distributed spring constant for the spring-dashpot model is then $s \approx 6 \times 10^6$ (N/m)/m using

$$s = \frac{1}{b}\,\frac{1}{\gamma(1-\gamma)}\,\frac{n_H\,\pi a_H^2\,E_H}{l_H}. \qquad (7)$$

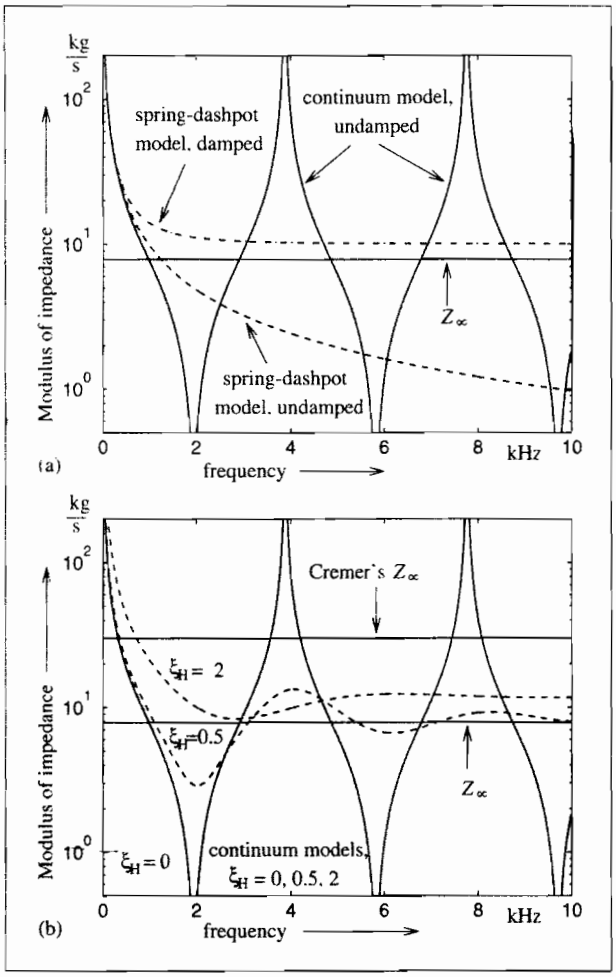

Figure 3. Frequency responses (moduli of the point input impedances) of various bow models. The numerical values refer to a (point and not a distributed) violin bow. Solid lines in both figures: the infinite loss-free transmission line (Z_∞) and the undamped continuum model. (a) Dashed line: the spring-dashpot model undamped. Dash-dot line: the spring-dashpot model damped. (b) Dashed lines: the continuum model with varying loss factor. Additional solid line: the infinite loss-free transmission line assumed by Cremer.

The distributed input impedance z_∞ according to equation (5) is $z_\infty = 790$ (kg/s)/m. The available damping data are not sufficient to cover the entire frequency range encountered on the bowed string. As an extrapolation for higher frequencies it will be assumed that the damping constant is independent of frequency. The damping constant of a single hair of 0.3 m length is $D \approx 0.1$ kg/s (Figure 2(b)) and that of a hair of 0.65 m length driven at its mid-point is $D \approx 0.2$ kg/s. The latter value gives $d = n_H D/b \approx 1000$ (kg/s)/m for the distributed damping constant. These numerical values of the distributed bow-hair parameters are given per unit width, and may be used for any actual bow width.

In view of the significant frequency dependence of the loss factor revealed by the measurements, it is hard to predict the value of the loss factor needed for the continuum model for high frequencies. We return to this issue shortly. The frequency response (the modulus of the impedance for $\gamma = 0.5$, multiplied by a bow width of $b = 10$ mm) predicted by the two models is shown in Figure 3. Two frequency responses are plotted in both figures for reference: that of the infinite loss-free transmission line, $Z_\infty = z_\infty b$, and that of the undamped continuum model which has alternating zeros and poles at radian frequencies $\omega = n\pi c_H/l_H$ with $n = 1, 2, 3....$ The logarithmic mean of the latter frequency response is Z_∞.

Figure 3(a) also shows the frequency response of the spring-dashpot model, with values of s and d as given above ("damped" case) and also with $d = 0$ ("undamped" case). In the damped case the impedance asymptotically approaches the value of the damping constant $D = d\,b$ for $\omega \to \infty$. In Figure 3(b) the frequency response of the continuum model is given for progressively increasing loss factor. The poles and zeros are removed and the response becomes smoother. A further solid line represents the frequency response of the infinite loss-free transmission line assumed by Cremer [3] in his discussion of the effect of longitudinal bow-hair compliance. The value quoted for a mono-layer violin bow, $Z_\infty = 30$ kg/s, is erroneously high and led Cremer to believe that bow-hair compliance was of little relevance to the contact mechanics of the bowed string. The numerical value is based on an unfortunate error in Schumacher [11] where $Z_\infty = 0.6$ kg/s for a single hair is given but $Z_\infty = 0.15$ kg/s is intended [18]. The latter value, derived from the longitudinal phase velocity and the mass per unit length, is in accordance with the present results. In Figure 3(b) it is clearly seen that the value of the bow-hair impedance Cremer assumed lies outside the range of any plausible mechanical model of the bow-hair behaviour. This erroneous value and the conclusion drawn from it have unfortunately been reproduced by other authors [19, 20].

Both models have been applied to the Eisenberg-Cremer reflection and transmission experiment. Predictions computed with the spring-dashpot model using the numerical values given above agree well with the experimental results, as will be seen in Section 3. With the apparently more realistic continuum model the results were much less convincing. To obtain reasonable agreement with the experimental results, a loss factor of the order of $\xi_H = 2$ had to be assumed. Even then the agreement was less good than with the spring-dashpot model. A damping factor this high is physically implausible, and we can only conjecture that in the Eisenberg-Cremer experiment frictional loss due to differential hair motion may have played a significant role. For the present investigation we simply observe that the spring-dashpot model performs well, and has the virtue of being very convenient for a numerical approach to the simulation of the bowed string. Therefore equation (3) will be employed whenever a constitutive equation is required.

For *point-bow* models the distributed quantities s and d are simply multiplied by the bow width. The constitutive relation becomes

$$F(t) = -\left(S\,\eta_H(t) + D\,\frac{\mathrm{d}\eta_H(t)}{\mathrm{d}t}\right) \qquad (8)$$

where F, S and D are lumped quantities and η_H is the bow-hair displacement at the point of contact. Based on the value

ACUSTICA · acta acustica
Vol. 84 (1998)

for the bow width of $b = 10$ mm used above, the lumped values are $S = 6 \times 10^4$ N/m and $D = 10$ kg/s for the violin bow.

For reference some results of this section are collected in Table I. The mass M_H is the mass of the ribbon of bow-hair at length l_H, the distance between frog and tip. The values M_H quoted here are derived from those of commercially available, ready-made hanks of hair [21] and take into account that the original hank is longer than l_H. The number of hairs $n_0 = 200$ of the violin bow is an estimate based on measurements of the mass of the hanks, the bow-hair density and diameter, and is consistent with the available data in the literature. The corresponding numbers of hairs for viola, cello and double-bass bows are derived by comparison of their values of M_H and l_H with those of the model violin-bow hank. It appears that the ribbons of bow-hair for the four types of bows differ little with respect to their thickness: a ribbon consists of roughly four layers of bow-hair.

All quantities pertaining to the bow-hair impedance are given as point-bow data and assume bowing at the bow midpoint ($\gamma = 0.5$). For finite-width calculations one may simply divide these values by the value of the average bow width given in the second column. The quantities S and D refer to the lumped spring-dashpot model of equation (8). The scaling for viola, cello and bass bows uses hair length l_H and bow width b. The impedance Z_∞ is calculated on the basis of equation (5). The last column gives approximate ranges of transverse characteristic impedances Z_0 for strings. These values are compiled from published data [22, 23, 24]. The comparison of the variation in bow and string impedance casts a shadow ahead: the nature of the bow and string contact must be expected to differ considerably across the range of bowed instruments.

3. Model of the contact area

In this section the mathematical model of the contact between string and bow will be developed. The point of departure for this investigation is, as stated above, the concept of reflection, transmission and scattering of waves travelling on a string and interacting with a bow at rest. The problem can be treated adequately as a linear problem. This allows the use of analytical methods and straightforward interpretation of experimental results.

For the purpose of the present investigation, we will focus on the motion of the string in the bowing plane, the plane in which string and bow-hair lie. Motion in the perpendicular plane may also play a role in the detailed response of a *bowed* string, but in the context of the present problem such effects can be safely neglected. The effects of the non-uniformity of the distribution of the bow force due to the static deformation bow-hair and string in the perpendicular plane will be discussed in Part III of this study.

Since most of the commonly-used models of the bowed string assume a point bow it is worth investigating first how the various ingredients for the model of the contact mechanics come into play in a point-bow model (Section 3.1). We use Cremer's rigid point-bow model as a starting point and then allow for longitudinal bow-hair compliance. In Section 3.2 the new, finite-width model for the contact area is developed. Again, a model assuming a rigid bow is considered first, and then the model is extended to include bow-hair compliance.

Table II. Details of the four model strings used for the parameter study: fundamental frequency ν_0, diameter $2a$, string length l and transverse characteristic impedance Z_0. Unless otherwise stated, $Z_T/Z_0 = 1.6$, $c_T/c_0 = 2.4$ and $b_S = 0.1$.

No.	Type	ν_0 [Hz]	$2a$ [mm]	l [m]	Z_0 [kg/s]
1	violin A	440.0	0.68	0.329	0.2
2	viola G	196.0	1.0	0.365	0.3
3	cello G	98.0	1.3	0.685	0.7
4	bass E	41.2	4.2	1.060	3.5

The strings in use on bowed instruments span a large range in the parameter space, as can be seen for example from the transverse characteristic impedances Z_0 given in Table I, and correspondingly a wide range of behaviour is found. It is not easy to make general observations valid for all combinations of strings and bows. The approach adopted here is to display the frequency dependence of reflection and transmission coefficients for a set of four model strings which have been chosen to represent as well as possible the range of behaviour of real strings. Details of these four model strings, one from each instrument of the violin family, are given in Table II.

Exact multiples of the fundamental frequency will be referred to by the harmonic number n. The reflection and transmission curves of each of the four model strings will be plotted versus n. Bending stiffness will be discussed in terms of Schelleng's [25] measure of inharmonicity b (denoted b_S here for clarity), the inharmonicity in cents in the nth mode per square of the harmonic number n. Schelleng suggests that the inharmonicity so defined should not exceed 0.1; in order not to underestimate the influence of bending stiffness, we will show results with $b_S = 0.1$ but will also consider the case of $b_S = 1$. In all examples, unless otherwise stated, the ratio of torsional to transverse characteristic impedance, defined below, is set to $Z_T/Z_0 = 1.6$. The ratio of torsional to transverse phase velocity is set to $c_T/c_0 = 2.4$. The dimensions of the model bows are adjusted to the particular instruments, violin-bow dimensions for the violin string and so on, as detailed in Table I.

3.1. Point-bow models

Assume in the first instance a perfectly rigid point bow, dividing an infinitely long string at the point $x = 0$ into two semi-infinite sections. Let the string have tension T, bending stiffness B, torsional stiffness K, mass and polar moment of inertia per unit length m and Θ respectively. (For a solid string of homogeneous material with shear modulus G, Young's modulus E and radius a, $K = G\pi a^4/4$, $B = E\pi a^4/4$.) The equations of motion for free transverse

Table I. Bow data used in modelling. For reference in the last column transverse characteristic impedance Z_0 of strings. See text.

Type	n_0	M_H [g]	l_H [m]	b [mm]	S [N/m]	D [kg/s]	Z_∞ [kg/s]	Z_0 (strings) [kg/s]
violin	200	4.5	0.65	10	6×10^4	10	7.9	0.2–0.4
viola	230	5.2	0.65	10	6×10^4	10	7.9	0.2–0.5
cello	290	6.2	0.61	13	11×10^4	18	10	0.4–1.1
bass	400	7.5	0.53	16	19×10^4	31	28	1.4–5.5

and torsional motion are

$$T\frac{\partial^2\eta}{\partial x^2} - B\frac{\partial^4\eta}{\partial x^4} = m\frac{\partial^2\eta}{\partial t^2} \tag{9}$$

$$K\frac{\partial^2\lambda}{\partial x^2} = \Theta\frac{\partial^2\chi}{\partial t^2} \tag{10}$$

as usual. The transverse displacement of the string in the bowing plane is denoted by η, and its angular displacement is denoted by χ (see Figure 4).

Provided the bow force is sufficiently high to prevent slipping the string can only roll against the bow, and this rolling constraint couples the transverse and the torsional motion at the point of contact. Transverse wave energy can be scattered into torsional wave energy and vice versa. If an incident transverse or torsional propagating wave originating from $x < 0$ impinges on the bow, six wave types are generated: a reflected and a transmitted transverse propagating wave, a reflected and a transmitted transverse evanescent wave, and a reflected and a transmitted torsional propagating wave. We present details for the case of an incident transverse wave, but an incident torsional wave could be treated in exactly the same way.

Assuming linear wave theory and unit amplitude for the incident transverse wave, the appropriate wave ansatz for the propagating and evanescent transverse waves and the torsional waves is

$$\eta = \left(1\, e^{-ik_P x} + r_P\, e^{ik_P x} + r_E\, e^{ik_E x}\right) e^{i\omega t}$$

$$\chi = \frac{1}{a} r_T\, e^{ik_T x}\, e^{i\omega t}$$

for $x \le 0$, and

$$\eta = \left(t_P\, e^{-ik_P x} + t_E\, e^{-ik_E x}\right) e^{i\omega t}$$

$$\chi = \frac{1}{a} t_T\, e^{-ik_T x}\, e^{i\omega t}, \tag{11}$$

for $x \ge 0$ where r_P, r_E and r_T are the (unknown) wave amplitudes for the reflected transverse propagating (subscript $_P$), the reflected transverse evanescent (subscript $_E$) and the reflected torsional (subscript $_T$) wave respectively. Correspondingly t_P, t_E and t_T are the (unknown) wave amplitudes of the transmitted waves. The wavenumbers k_P and k_E are respectively the pure real and pure imaginary roots of the dispersion relation for transverse waves

$$\omega^2 - \frac{T}{m}k^2 - \frac{B}{m}k^4 = 0, \tag{12}$$

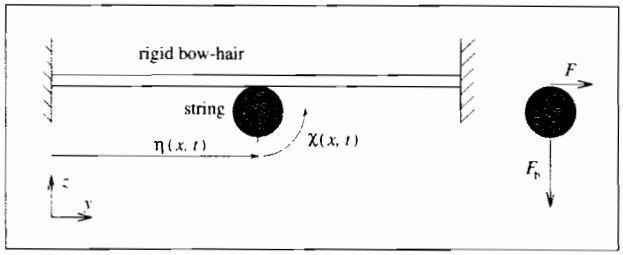

Figure 4. Schematic representation of the mechanical model for the rigid bow, and definition of coordinates. The friction force F acts in the *bowing plane*, the (normal) bow force F_b acts in the *perpendicular plane*.

and k_T is the solution of the dispersion relation for torsional waves

$$\omega^2 - \frac{K}{\Theta}k^2 = 0. \tag{13}$$

(The convention used is that $k_E = -i\alpha$ where α is a positive real quantity.) The frequency-dependent behaviour of k_P^2, k_E^2 and k_T^2 is shown in Figure 7 below.

Seven equations are needed to determine the six (in general complex) amplitudes of these reflected and transmitted waves and the amplitude of the friction force at the point of contact F. These equations arise from the six jump conditions and the rolling constraint at the point of contact $x = 0$:

$$\left[\eta\right]_{-0}^{+0} = 0 \qquad \left[\eta_x\right]_{-0}^{+0} = 0$$

$$\left[\eta_{xx}\right]_{-0}^{+0} = 0 \qquad \left[\chi\right]_{-0}^{+0} = 0$$

$$B\left[\eta_{xxx}\right]_{-0}^{+0} = F \qquad K\left[\chi_x\right]_{-0}^{+0} = aF$$

$$\eta = a\chi. \tag{14}$$

Derivatives with respect to x are denoted by subscript $_x$. Assuming the above wave ansatz equations (11), this system of equations can be solved straightforwardly (if a little tediously). The results for r_P, r_T and F are:

$$r_P = \frac{-1}{\left(1 + \frac{Z_S}{Z_T}\right)\left(1 + \frac{k_P}{k_E}\right)}, \tag{15}$$

$$r_T = \frac{\frac{Z_S}{Z_T}}{1 + \frac{Z_S}{Z_T}}, \qquad F = \frac{-i\omega 2 Z_S}{1 + \frac{Z_S}{Z_T}}. \tag{16}$$

The transverse and torsional characteristic impedances of the string are

$$Z_S = m\omega\left(\frac{1}{k_P} - \frac{1}{k_E}\right) \quad \text{and} \quad Z_T = \frac{c_T\Theta}{a^2}, \tag{17}$$

ACUSTICA · acta acustica
Vol. 84 (1998)

respectively, where $c_T = (K/\Theta)^{1/2}$ is the torsional phase velocity. The amplitude of the transmitted transverse propagating wave is $t_P = 1 + r_P$. The torsional reflection and transmission coefficients are identical in amplitude, since both are generated by the same friction force applied at the "bowed" point and the torsional behaviour is entirely symmetric about that point. The amplitudes of the (evanescent) near-fields are $r_E = t_E = (k_P/k_E)\, r_P$.

In the limit of vanishing bending stiffness it can be shown that

$$\lim_{B\to 0} \frac{k_P}{k_E} = 0 \quad \text{and} \quad \lim_{B\to 0} Z_S = Z_0 = c_0 m\,, \qquad (18)$$

where $c_0 = (T/m)^{1/2}$ and Z_0 are respectively the transverse phase velocity and characteristic impedance for the free, perfectly flexible string. Formally, application of equations (18) in equations (15) leads to expressions for the reflection and transmission coefficients for the case of the perfectly flexible string:

$$r_P = \frac{-1}{1 + \frac{Z_0}{Z_T}}\,, \qquad (19)$$

$$r_T = \frac{\frac{Z_0}{Z_T}}{1 + \frac{Z_0}{Z_T}}\,, \qquad F = \frac{-i\omega 2 Z_0}{1 + \frac{Z_0}{Z_T}}\,. \qquad (20)$$

However, the underlying equations of motion and the jump conditions for this case are fundamentally different from those for the stiff case. Without bending stiffness there are no evanescent waves. The jump conditions in η_{xx} and η_{xxx} carry no information. Instead $T\left[\eta_x\right]_{-0}^{+0} = -F$.

In the limits of the perfectly flexible string and the rigid bow, the reflection and transmission coefficients are determined solely by the kinematics of rolling, through the ratio Z_T/Z_0, and are *independent* of frequency. This is seen in Figure 5(a) where the reflection and transmission coefficients r_P and t_P are plotted versus harmonic number n. As the impedance ratio Z_T/Z_0 is the same for all four model strings, their reflection and transmission curves collapse.

The solution for the perfectly flexible case is also the limiting solution for the stiff case in the limit of $\omega \to 0$, since

$$\lim_{\omega\to 0} \frac{k_P}{k_E} = 0 \quad \text{and} \quad \lim_{\omega\to 0} Z_S = Z_0 = c_0 m\,. \qquad (21)$$

In fact the asymptotic behaviour of the reflection and transmission coefficients for $\omega \to 0$ does not depend on the details of the model for any of the models discussed here, provided the modulus of the bow impedance is infinite for $\omega \to 0$. In other words, for $\omega \to 0$ the conventional model of a perfectly flexible string and a rigid point-bow is as good as any model. The details of the particular model determine the deviations at higher frequencies from the frequency-independent "kinematical" values of the conventional model.

In Figure 5(b) the reflection and transmission coefficients r_P and t_P for the model of the *stiff* string on the rigid point bow are given. The inharmonicity parameter, $b_S = 0.1$, is the same for all four strings causing the curves describing

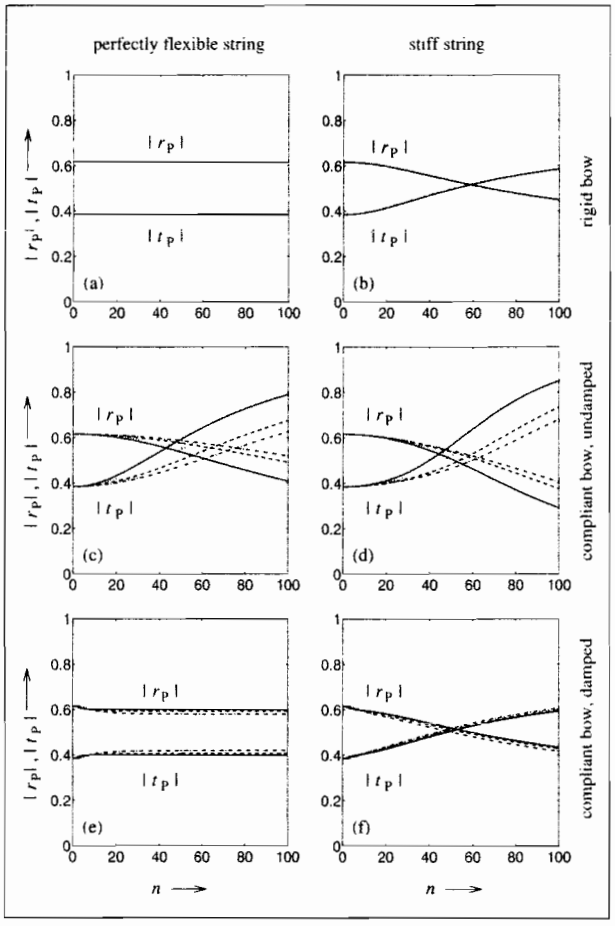

Figure 5. Transverse reflection and transmission coefficients computed with point-bow models, versus harmonic number n. Column 1: perfectly flexible string. Column 2: stiff string. Rows 1–3: rigid, undamped compliant and damped compliant bow model. Bow-hair compliance for the set of four model bows according to Table I, columns S and D. Solid, dashed, dash-dot and dotted lines represent the four strings of Table II in numerical order. (For real musical strings, the model used here may not necessarily be accurate for very high values of n.)

the reflection and transmission behaviour to collapse. As the frequency increases a greater fraction of the incident wave energy is transmitted through the bow. Increased bending stiffness facilitates transmission. This is the effect discussed by Cremer [3], in which the finite bending stiffness of the string allows progressive "tunnelling" of energy past the "bowed" point as frequency rises.

When the longitudinal compliance of the bow-hair is included in the model the jump conditions characterising the model system remain the same. With coordinates defined as in Figure 6 the rolling constraint becomes

$$\eta = a\,\chi + \eta_H\,. \qquad (22)$$

The additional unknown η_H is catered for by a constitutive relation for the bow-hair behaviour, here in a point-bow version. The formal solution with unspecified bow-hair impedance Z_H, however, remains the same for any constitutive relation.

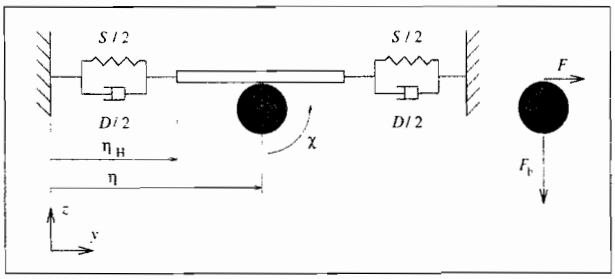

Figure 6. Schematic representation of the mechanical model for the compliant bow assuming the spring-dashpot model, and definition of coordinates.

Solving these equations using the wave ansatz equation (11), the formulae for the transverse and torsional reflection coefficients and the friction force are now:

$$r_{\mathrm{P}} = \frac{-1}{\left(1 + \frac{Z_{\mathrm{S}}}{Z_{\mathrm{T}}} + \frac{2Z_{\mathrm{S}}}{Z_{\mathrm{H}}}\right)\left(1 + \frac{k_{\mathrm{P}}}{k_{\mathrm{E}}}\right)}, \tag{23}$$

$$r_{\mathrm{T}} = \frac{\frac{Z_{\mathrm{S}}}{Z_{\mathrm{T}}}}{1 + \frac{Z_{\mathrm{S}}}{Z_{\mathrm{T}}} + \frac{2Z_{\mathrm{S}}}{Z_{\mathrm{H}}}}, \quad F = \frac{-\mathrm{i}\omega 2 Z_{\mathrm{S}}}{1 + \frac{Z_{\mathrm{S}}}{Z_{\mathrm{T}}} + \frac{2Z_{\mathrm{S}}}{Z_{\mathrm{H}}}}. \tag{24}$$

As in the rigid case the transverse transmission coefficient is $t_{\mathrm{P}} = 1 + r_{\mathrm{P}}$, the near-field amplitudes are $r_{\mathrm{E}} = t_{\mathrm{E}} = (k_{\mathrm{P}}/k_{\mathrm{E}})\, r_{\mathrm{P}}$, and the two torsional coefficients are identical. As above the corresponding formulae for the perfectly flexible string are obtained by setting $Z_{\mathrm{S}} = Z_0$ and $k_{\mathrm{P}}/k_{\mathrm{E}} = 0$.

For the results seen in Figures 5(c)–(f) the bow-hair impedance has been specified according to $Z_{\mathrm{H}} = -\mathrm{i}S/\omega + D$, the spring-dashpot model discussed in Section 2. Figures 5(c)–(d) show the reflection and transmission coefficients behaviour for the four model strings, in contact with bows with spring stiffnesses S as given in Table I but with the damping $D = 0$. Figures 5(e)–(f) show the corresponding results with damping values D according to Table I.

Only on an elastic bow can strings with identical $Z_{\mathrm{S}}/Z_{\mathrm{T}}$ show differences in behaviour. The solid, dashed, dash-dot and dotted lines correspond to the violin, viola, cello and double-bass strings of Table II, respectively. The bow-hair elasticity has no effect for $\omega \to 0$, but otherwise it is clear that it has a very significant influence. It leads to a more transparent bow and to lower torsional coefficients. The effects of bow-hair elasticity are smaller if the bending stiffness of the string is high.

Damping, seen in Figures 5(e)–(f), leads to a stronger mismatch of string and bow impedances and the bow can resemble a rigid bow to a certain degree. This in turn means that bending stiffness plays a greater role in the dispersive behaviour. Energy dissipation is significantly higher for lower strings. The differences in reflection and transmission behaviour may seem small when the coefficients are plotted versus harmonic number, but are considerable when the coefficients are plotted versus frequency: in our example the fundamental frequencies of the model strings lie more than an order of magnitude apart. The fact that the bows for the lower instruments of the violin family are stiffer than the violin bow counters the spread in reflection and transmission behaviour somewhat. As we will see below, the spread is significantly larger in finite-width models.

The strong changes in the frequency dependence brought about by bow-hair compliance are in contrast to a discussion by Cremer [3], who argues that the mechanical properties of the bow-hair do not matter for the motion of a bowed string and that the assumption of a rigid bow is sufficiently accurate. Cremer discusses the possible influence of bow compliance on the basis of the point input impedance of an infinite elastic (loss-free) transmission line, $Z_{\mathrm{H}} = Z_\infty$ in our notation. However, firstly, this quantity is frequency independent, and can therefore not describe the details of the influence of the bow properly. Secondly, the value quoted for the violin bow, $Z_\infty = 30$ kg/s, is erroneously high as was pointed out in Section 2.

3.2. Finite-width models

Even if in some cases a rigid point-bow model may be an adequate approximation to the actual bowed string, the assumption of a rigid bow is, however, not at all acceptable when modelling a bow of finite width.

3.2.1. Governing equations

For such a finite-width bow the friction force is distributed across the bow. The governing equations for the motion of the section of string in contact with the distributed bow-hair are the equations of momentum (25) and angular momentum (26), coupled through the friction-force term $f(x,t)$ common to both:

$$T\frac{\partial^2 \eta}{\partial x^2} - B\frac{\partial^4 \eta}{\partial x^4} + f = m\frac{\partial^2 \eta}{\partial t^2}, \tag{25}$$

$$K\frac{\partial^2 \chi}{\partial x^2} - a f = \Theta\frac{\partial^2 \chi}{\partial t^2}. \tag{26}$$

If the bow is modelled as a rigid support then these equations together with the rolling constraint

$$\eta(x,t) = a\,\chi(x,t) \tag{27}$$

constitute a system of three linear equations for which analytical, travelling-wave solutions can be sought. Solving the system of linear equations for sticking/rolling with the wave ansatz

$$(\eta, \chi, f) = (\eta_0, \chi_0, f_0)\, e^{\mathrm{i}\omega t - \mathrm{i}kx}, \tag{28}$$

where η_0, χ_0 and f_0 are complex amplitudes, yields the dispersion relation

$$\omega^2 - \frac{c_0^2 m + c_{\mathrm{T}}^2\,\Theta/a^2}{m + \Theta/a^2}\,k^2 - \frac{B}{m + \Theta/a^2}\,k^4 = 0, \tag{29}$$

with c_0 and c_{T} as defined above. This can be rewritten in a simple form as

$$\omega^2 - c_{\mathrm{roll}}^2\,k^2 - A\,k^4 = 0 \tag{30}$$

ACUSTICA · acta acustica
Vol. 84 (1998)

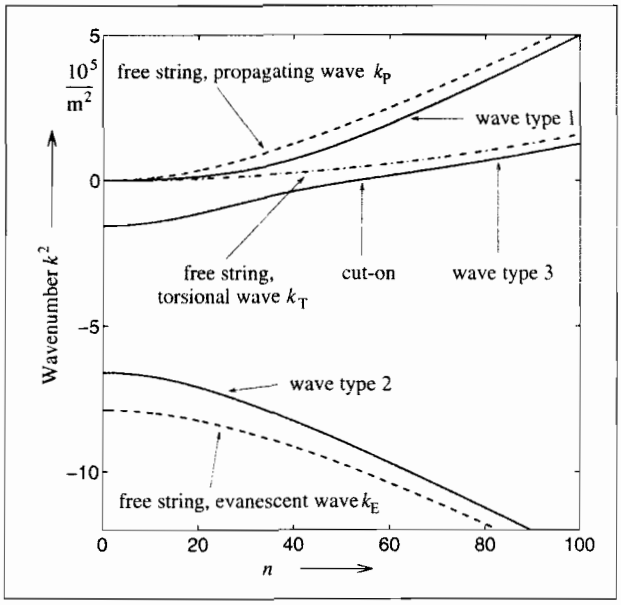

Figure 7. Wavenumbers squared characterising the motion of the string versus harmonic number n. Dashed lines: wavenumbers for transverse waves on free (stiff) string. Dash-dot line: wavenumber for torsional wave on free string. Solid lines: string rolling on compliant undamped support. Wave type 3 is only present on compliant supports. Note the cut-on. String No.1 from Table II and violin bow according to Table I.

with

$$c_{\text{roll}}^2 = \frac{c_0^2\, m + c_T^2\, \Theta/a^2}{m + \Theta/a^2} = c_0^2\, \frac{1 + \frac{Z_T}{Z_0}\frac{c_T}{c_0}}{1 + \frac{Z_T}{Z_0}\frac{c_0}{c_T}}\,, \tag{31}$$

$$A = \frac{B}{m + \Theta/a^2}\,. \tag{32}$$

The velocity c_{roll} is the frequency-independent phase velocity of a mixed transverse/torsional wave propagating on a perfectly flexible string rolling on a rigid surface. The value of c_{roll} lies between that of the transverse phase velocity for the perfectly flexible free string, c_0, and that of the torsional phase velocity, c_T. Measured values of the velocity ratio c_T/c_0 lie in the range of 2–8 [14]. For a homogeneous string $Z_T/Z_0 = 0.5\, c_T/c_0$, and for any wrapped string with wrapping density higher than core density, $Z_T/Z_0 > 0.5\, c_T/c_0$; therefore usually $c_{\text{roll}} > c_0$.

The stiff string rolling on a rigid surface shows dispersive behaviour. From the dispersion relation equation (30) one may compute two wavenumbers, k_1 and k_2, corresponding to a propagating and an evanescent wave like those on the free stiff string. The propagating wave shows behaviour similar to that of the rolling wave of the perfectly flexible string. Its phase velocity is $c > c_{\text{roll}}$ due to the effects of bending stiffness. The evanescent wave has a wavenumber with a much higher magnitude than the evanescent wave on the free stiff string. The asymptotic value of this wavenumber for $\omega \to 0$ is readily calculated to be

$$\lim_{\omega\to 0} k_2 = \pm \mathrm{i} \left(\frac{T}{B}\right)^{1/2} \left(1 + \frac{Z_T}{Z_0}\frac{c_T}{c_0}\right)^{1/2} \tag{33}$$

instead of

$$\lim_{\omega\to 0} k_E = \pm \mathrm{i} \left(\frac{T}{B}\right)^{1/2} \tag{34}$$

for the free stiff string.

When the bow is not rigid, the procedure must be modified slightly. Now the model of behaviour for the bow-hair provides a fourth equation via the constitutive relation describing the compliance of the support, equation (1) or any other constitutive relation. The rolling constraint is modified to

$$\eta(x,t) = a\,\chi(x,t) + \eta_H(x,t)\,. \tag{35}$$

Provided the constitutive relation is linear, this again gives a system of linear equations for which analytical, travelling-wave solutions can be found. Using an ansatz like equation (28) with an additional fourth component η_H leads to a dispersion relation of sixth order in k and fourth order in ω, which after some manipulation takes the following form:

$$\left(\omega^2 - c_0^2\, k^2 - \frac{B}{m}\, k^4\right)\left(\omega^2 - c_T^2\, k^2\right) - \left(\omega^2 - c_{\text{roll}}^2\, k^2 - A\, k^4\right)\frac{m + \Theta/a^2}{m\Theta/a^2}\, \mathrm{i}\omega z_H = 0\,. \tag{36}$$

The first and second bracketed expressions are the dispersion relations characterising the transverse and the torsional motion of the free string, the third bracketed expression is the dispersion relation of the stiff string rolling on the rigid support. The full equation is bi-cubic and therefore has three roots in k^2.

The wavenumbers of the three wave types which result from the dispersion relation are displayed in Figure 7 as solid lines. As before the bow is represented by the spring-dashpot bow-model ($z_H = -\mathrm{i}s/\omega + d$). Damping is neglected at first. The particular choice of parameters of bow and string for the example shown in Figure 7 leads to three real roots in k^2. Higher values of bending stiffness would result in a regime with one real and two complex conjugate roots in k^2.

For $\omega \to \infty$ these three wave types can readily be identified with well-known wave types. Wave type 1 is a transverse propagating wave and corresponds to the transverse propagating wave on the free stiff string; wave type 2 is a transverse evanescent wave and corresponds to the usual evanescent wave on the free stiff string; wave type 3 corresponds to the torsional wave on the free string. In other words, for $\omega \to \infty$ the elastic support is completely transparent and the string behaves like a free string.

At the opposite end of the spectrum, $\omega \to 0$, wave type 1 can be identified as the rolling wave which was discussed in the context of the rigid support (equation(31)). Wave types 2 and 3 behave similarly to the two wave types corresponding to a simpler equation, equation (45). This equation describes the transverse motion (no rotational motion) of a stiff string on an elastic (Winkler) foundation. Cut-on of wave type 3, marked in Figure 7, takes place at radian frequency

$$\omega_c = \left(\frac{s}{m} + \frac{s}{\Theta/a^2}\right)^{1/2}. \tag{37}$$

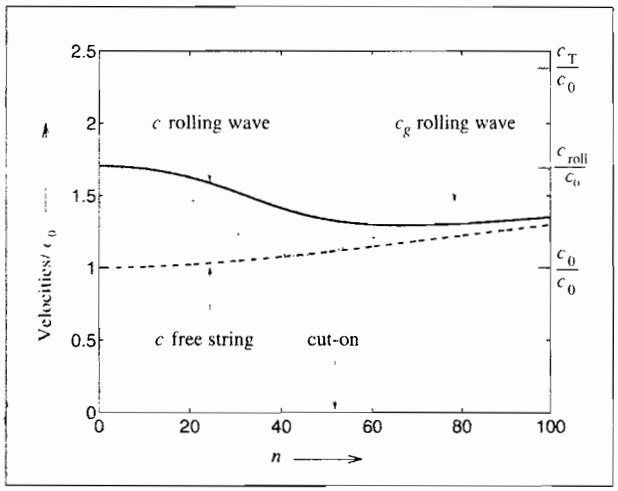

Figure 8. Phase and group velocities versus harmonic number n. Solid line: phase velocity of rolling wave on compliant support. Dotted line: group velocity of rolling wave on compliant support. Dashed line: phase velocity of transverse wave on free string. String No.1 from Table II.

For a homogeneous string $\omega_c = (3\,s/m)^{1/2}$. The cut-on frequency is not affected by bending stiffness.

A brief discussion of the dispersive behaviour of these waves is of interest: Figure 8 shows the phase and group velocity as a function of frequency. On a rigid support, a perfectly flexible string has a phase velocity $c = c_{\text{roll}}$, independent of frequency. For a stiff string, the phase velocity is $c = c_{\text{roll}}$ for $\omega \to 0$ and increases with frequency. The relative increase in c due to bending stiffness is smaller for the rolling string than for the free string. On a compliant support perfectly flexible and stiff strings show the same qualitative behaviour. The phase velocity of wave type 1 is $c = c_{\text{roll}}$ for $\omega \to 0$. It decreases first and then asymptotically approaches the phase velocity of the corresponding free string as $\omega \to \infty$. Wave type 3 only propagates from its cut-on frequency onwards. Its phase velocity is infinite at cut-on and asymptotically approaches the phase velocity of the torsional wave.

Damping turns previously real and imaginary wavenumbers complex. There is then no longer a clear cut-on frequency for wave type 3, although the main characteristics of the system remain.

3.2.2. Reflection and transmission

Returning now to the reflection and transmission problem, we must link a section of string in contact with the bow to two semi-infinite sections of free string, and find the correct jump conditions at the interfaces of these three sections and the wave ansatz satisfying these conditions. The compliant finite-width bow follows after dealing with the rigid case. Bending stiffness is allowed for.

A transverse wave incident on the bow generates, on each side of the bow, two outgoing transverse waves, (one propagating, one evanescent) and an outgoing torsional wave. From the analysis of the dispersive behaviour of the string rolling on the rigid support above, it follows that under the bow there are four waves to be considered, two wave types in two directions. In total there are 10 unknown wave amplitudes. Assuming there were no singular forces at the interfaces we would find the following jump conditions at each interface, at $x = 0$ and at $x = b$:

$$\begin{aligned} \left[\,\eta\,\right]^+_- &= 0, & \left[\eta_x\right]^+_- &= 0, \\ \left[\eta_{xx}\right]^+_- &= 0, & \left[\,\chi\,\right]^+_- &= 0, \\ \left[\eta_{xxx}\right]^+_- &= 0, & \left[\,\chi_x\,\right]^+_- &= 0\,. \end{aligned} \tag{38}$$

But this gives two conditions too many: 12 conditions for 10 unknown wave amplitudes. We can deduce that singular edge forces at the interfaces, unknowns of the problem, are inevitable in a rigid bow model. The correct fifth and sixth jump conditions are then

$$\begin{aligned} B\left[\eta_{xxx}\right]^+_- &= F\,, \\ K\left[\,\chi_x\,\right]^+_- &= a\,F\,, \end{aligned} \tag{39}$$

where the edge force is $F\,\delta(x)$ or $F\,\delta(x-b)$ as appropriate. Note that the rolling constraint no longer provides a condition at the interface, as it is already incorporated into the solution of the equations of motion under the bow.

To solve the sets of equations arising from the above jump conditions we use an ansatz equivalent to that for the point bow (equations (11)) for the waves on either side of the bow. For the four waves under the bow ($0 \le x \le b$) an additional ansatz is needed:

$$\begin{aligned} \eta &= \left(t_1\,e^{-\mathrm{i}k_1 x} + t_2\,e^{-\mathrm{i}k_2 x}\right)\,e^{\mathrm{i}\omega t} \\ &\quad + \left(r_1\,e^{\mathrm{i}k_1 x} + r_2\,e^{\mathrm{i}k_2 x}\right)\,e^{\mathrm{i}\omega t}\,, \\ \chi &= \frac{1}{a}\,\eta(x,t)\,, \end{aligned} \tag{40}$$

where t_1, t_2 and r_1, r_2 are the (unknown) wave amplitudes of the waves under the bow and k_1 and k_2 are the right-going solutions to the dispersion relation equation (29). The wave ansatz is needed in two versions, one for η and one for χ as both displacements occur in the jump conditions.

Substitution leads to a set of 12 linear equations for the 10 wave amplitudes and the two edge forces. A typical example of the resulting force distribution under the bow is displayed in Figure 9(a). It consists of singular friction forces at the edges of the bow and a distributed friction force in the interior of the contact area. These two contributions are separated in Figure 9(a), for clarity. The singular forces are spread into rectangular bars (of correct area), and the distributed force is shown as a separate curve. The distribution of the friction force is time and frequency dependent; a snapshot of the friction force at phase angle $\pi/4$ for the harmonic number 10 is displayed. Note that the wavelengths in these examples are an order of magnitude larger than the bow width. The spatial distribution of the friction force as shown is therefore not primarily due to differences in phase across the width of the bow.

ACUSTICA · acta acustica
Vol. 84 (1998)

If bow-hair compliance is allowed for, singular forces at the edges of the bow cannot occur. If they were to do so, the displacement of the edge bow-hairs would be infinite. This physical statement finds its mathematical counterpart in the fact that there are now six waves to be considered under the bow, three wave types in two directions; in total there are 12 unknown wave amplitudes. For the set of equations to be closed the edge forces must necessarily be zero. For the six waves under the bow ($0 \leq x \leq b$) the wave ansatz for η is:

$$\eta = \left(t_1 e^{-ik_1 x} + t_2 e^{-ik_2 x} + t_3 e^{-ik_3 x}\right) e^{i\omega t} + \left(r_1 e^{ik_1 x} + r_2 e^{ik_2 x} + r_3 e^{ik_3 x}\right) e^{i\omega t} . \quad (41)$$

The ansatz for the rotational component of the string motion under the bow requires an expression for the ratio χ/η, which is $\chi/\eta = 1/a$ in the rigid case but is frequency dependent here. It may be found by substituting the constitutive relation for the force term in the equation of angular momentum equation (26). This results in an expression giving η_H as a function of χ which is then used to eliminate η_H in the rolling constraint equation (35), leading to

$$\lambda = \frac{\chi}{\eta} = \frac{1}{a}\left[1 - (\omega^2 - c_T^2 k^2)\frac{\Theta/a^2}{i\omega z_H}\right]^{-1} . \quad (42)$$

This ratio χ/η has to be computed for each of the three solutions k_{1-3} of the dispersion relation. If the three ratios are labelled λ_{1-3}, the ansatz for the torsional displacement becomes

$$\chi = \left(\lambda_1 t_1 e^{-ik_1 x} + \lambda_2 t_2 e^{-ik_2 x} + \lambda_3 t_3 e^{-ik_3 x}\right) e^{i\omega t} + \left(\lambda_1 r_1 e^{ik_1 x} + \lambda_2 r_2 e^{ik_2 x} + \lambda_3 r_3 e^{ik_3 x}\right) e^{i\omega t} . \quad (43)$$

When the reflection and transmission calculation is now performed one finds that the singular forces generated by the rigid-bow model are spread out by the near-fields arising from bow-hair compliance. In other words, the interface of the free string and the string under the bow is more permeable to transverse waves. This effect is illustrated in Figures 9(b)–(d). The two curves represent the violin and double-bass model strings from Table II under the corresponding bows. In Figure 9(b) are shown cases with compliant bows with values for s and d 100 times higher than the measured values. The singular forces at the interfaces have been spread out to some extent. In Figure 9(c) we see the force distribution for model bows for which the values of s and d have been set to the values arising from the relevant measurements. The length-scale over which the edge forces are spread is now wider than the bow itself, so that there is no concentration of force at the interfaces. For this reason it was stated earlier that bow-hair compliance is essential in a finite-width model: the rigid bow model does not give a remotely reasonable approximation to this behaviour. The final example, Figure 9(d), is that of bows with very low values s and d. The friction force is very small. The overall trend for the usual values of s and d is that rather even force distribution is found for low frequencies of the incident wave, that is on the lower strings of the instruments of the violin family and on the higher strings for waves with low harmonic number. Locally high force levels can occur when the incident wave is of high frequency.

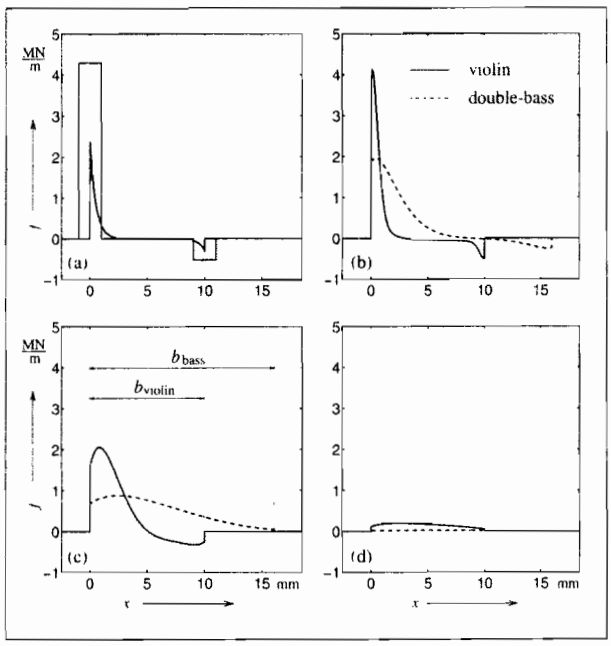

Figure 9. Friction force f (in MN/m) versus string coordinate x for incident transverse waves with unit amplitude and frequency corresponding to harmonic number $n = 10$. Strings according to Table II. (a) Rigid bow, violin string only. (b)–(d) Compliant bows, violin (solid) and double-bass (dashed) on corresponding strings: (b) with high values of s and d, 100 times the values given in Table I. (c) with the measured values of s and d given in Table I. (d) with low values of s and d, 0.01 times the values given in Table I. Note how the singular edge forces arising from the rigid bow (represented by vertical bars in (a)) are spread out progressively through the effects of increasing bow-hair compliance.

In Figures 10(a)–(f) examples of the reflection and transmission predictions for finite-width models are given. The six plots are organised in the same way as in Figure 5 for the point-bow models. The set of strings is also the same as in Figure 5. In Figures 10(a)–(b) we see the rigid bow models, first for the perfectly flexible strings and then for the stiff strings. The finite-width bow renders the system less permeable than a point bow: the singular force at the edge of a finite-width bow facing the incident wave alone is higher than the force obtained with the rigid point-bow model. Due to finite-width effects the curves for the different strings no longer collapse. In Figures 10(c)–(d) the predictions obtained from the undamped compliant bow models are presented. At high frequency the transverse transmission coefficient t_P is always higher than in the corresponding point-bow models.

In Figures 10(e)–(f) the predictions obtained from the damped compliant bow-models are presented. Finite-width models predict substantially higher losses than point-bow models: these are highest for the lower strings. If compliance is allowed for then the effect of bending stiffness is very small as long as Schelleng's [25] suggested limit is respected.

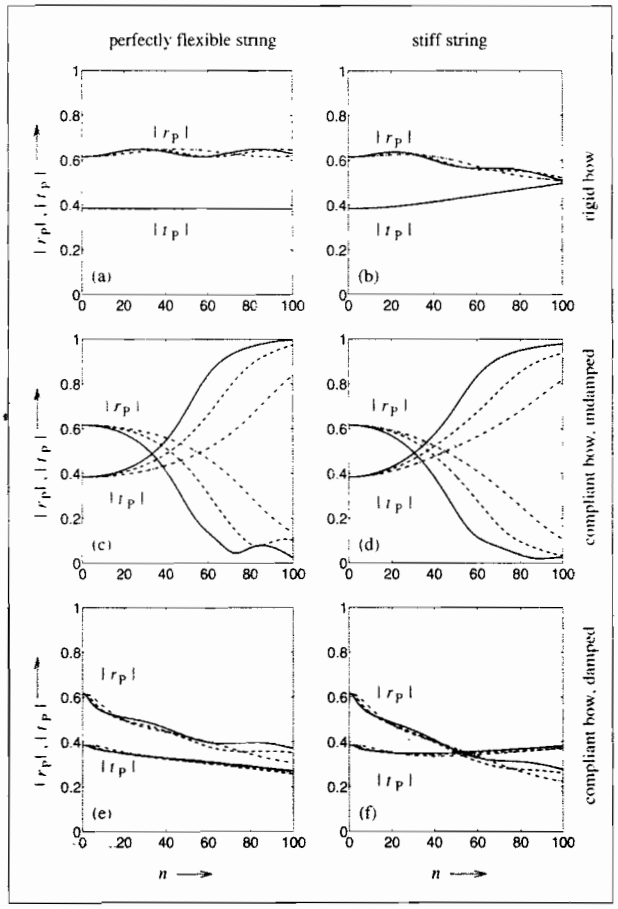

Figure 10. Transverse reflection and transmission coefficients computed with point-bow models, versus harmonic number n . Solid, dashed, dash-dot and dotted lines represent the four strings of Table II in numerical order. Column 1: perfectly flexible string. Column 2: stiff string. Rows 1–3: rigid, undamped compliant and damped compliant bow model. Bow-hair compliance for the set of four model bows according to Table I, columns S and D, and distributed over the given bow widths.

4. Comparison with experimental results

4.1. Experimental setup

The experimental results pertaining to this investigation are taken from a report produced by Eisenberg [4] under the supervision of Lazarus and Cremer. The results of only one experiment have been published by Cremer [3], page 129. The report contains more interesting findings than the participating researchers seem to have been aware of, and it is unfortunate that this work has not been made more widely available.

The experimental setup, briefly described by Cremer [3], consists of a long string (30 m) between two fixed ends. A bow is placed on the string between two velocity sensors. These sensors are simple electro-inductive devices consisting of loops of very thin copper wire glued to the surface of the string and placed between the two poles of a permanent magnet. Copper wires are attached to opposite sides of the string. For sufficiently small amplitudes of displacement the voltages induced in the loops are proportional to the surface velocity of the string at the observation point. Once calibrated, the sum of the induced voltages corresponds to the transverse velocity, the difference corresponds to the angular velocity. Transverse wave packets of sinusoidal content were generated at a point of the string between a termination of the string and a sensor.

Table III. Details of strings used by Eisenberg, Lazarus and Cremer in their experimental investigation of the reflection and transmission behaviour: diameter $2a$, transverse phase velocity at low frequency c_0, tension T, transverse impedance $Z_0 = T/c_0$, impedance ratio Z_T/Z_0 and Young's modulus E. An approximate identification with "real" strings, based on Z_0, would be 1: double-bass D (73 Hz); 2: double-bass B (31 Hz); 3: violin G (196 Hz); the frequencies in parentheses give the nominal tunings.

No.	$2a$ [mm]	c_0 [m/s]	T [N]	Z_0 [kg/s]	Z_T/Z_0	E [GPa]
1	3	266	554	2.08	2	2–4
2	3	160	886	5.54	2	130
3	1	429	143	0.33	–	2–4

Three strings were used: two nylon strings with diameters of 3 mm and 1 mm (string 1 and string 3), and one steel string with a diameter of 3 mm (string 2). The terminology used to describe the construction of these strings is ambiguous. Eisenberg refers to the strings as "Seile" (ropes). Cremer speaks of "Nylonsaite" (nylon string) and "Stahlseil" (steel rope). Cremer's translator speaks of both as "braided strings". Probably all the strings Eisenberg used, with the possible exception of the 1 mm string, were ropes, twisted and not braided. For each string experiments were undertaken applying two different tension forces, differing by a factor of 1.5–2, which produces six cases. In all cases a violin bow was placed on the string. In an additional run the bow-hair was replaced by a "rigid bow" consisting of a strip of nylon glued onto a strip of steel of width 4 mm. Details of the strings used in the cases selected for presentation here are given in Table III.

The transverse phase velocity c_0 and the string tension T were measured with good accuracy. The values of the transverse impedance in Table III are $Z_0 = T/c_0$. Based on these impedance values, approximate identifications of these strings with strings on real instruments are suggested. The torsional impedance Z_T was not measured. The measurement of the torsional phase velocity, from which one could have derived an approximate value of the torsional impedance, seems to have been regarded by Cremer as unreliable. One can, however, derive the impedance ratio Z_T/Z_0 from the low-frequency reflection and transmission behaviour as it has become apparent that for low frequencies the reflection and transmission behaviour depends almost solely on Z_T/Z_0. These are the values of Z_T/Z_0 given in Table III.

Eisenberg's measurements of the frequency dependence of the transverse phase velocity on the rather dispersive steel "string" enable us to determine the *in situ* value of the bending stiffness. We derive a value for the bending stiffness of this string corresponding to a Young's modulus of approximately $E = 130$ GPa, roughly two thirds of the usual value

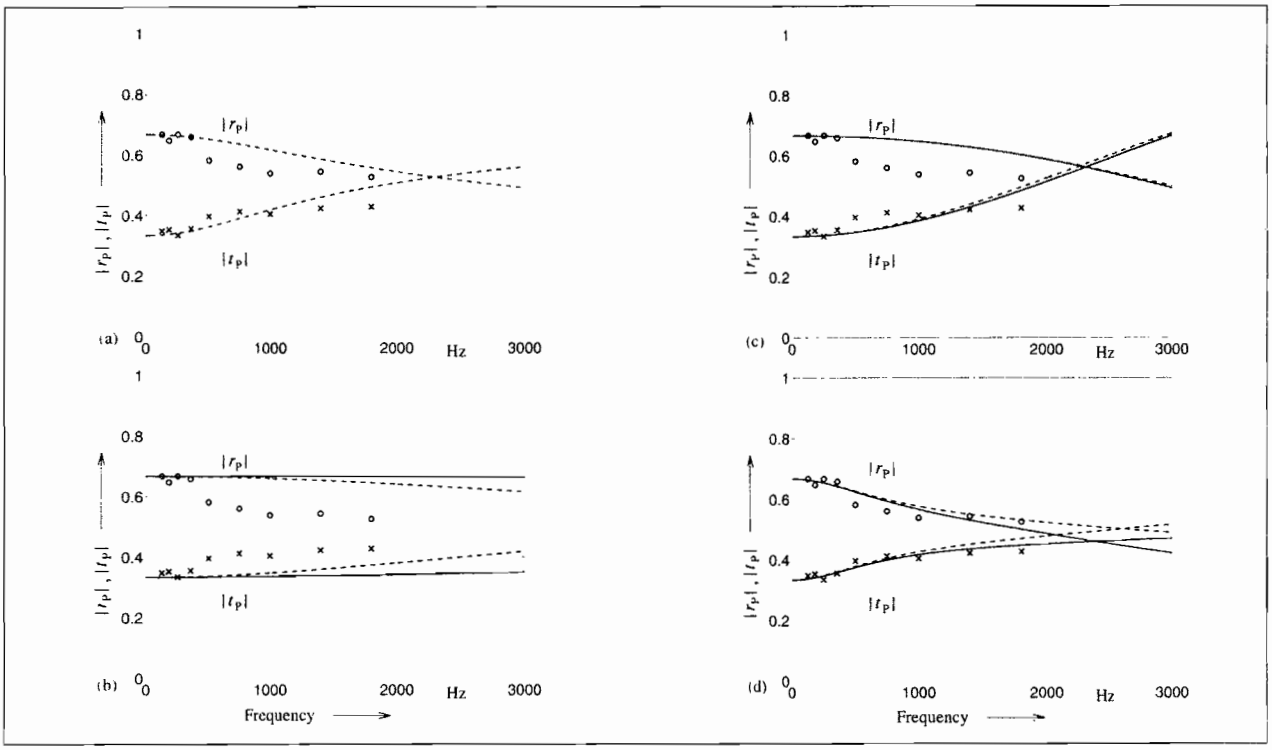

Figure 11. Transverse reflection and transmission coefficients from experimental and theoretical investigations for Eisenberg's string No.1 (3 mm nylon) versus frequency. Measured reflection (o) and transmission (x) coefficients. Solid lines: finite-width predictions. Dashed lines: point-bow predictions. (a) Cremer's rigid point-bow model with the *adjusted* Young's modulus of the string $E = 35$ GPa. (b) Rigid models, now with a *realistic* value $E = 4$ GPa. (c) Compliant models without damping. (d) Compliant models with damping.

for a homogeneous (bulk) sample of steel. For the less dispersive nylon strings we must resort to values of the Young's modulus taken from the literature. One finds values between $E = 2$–4 GPa. Herein the upper limit, $E = 4$ GPa, is chosen to ensure that the effect of bending stiffness is not underestimated.

In all cases preliminary experiments were used to find the minimum value of the bow force required to ensure that the reflection and transmission behaviour was independent of bow force. This was done to avoid slipping of the string on the one hand and strong deformation of the string under the bow force on the other. The frequency-dependent rate of damping for transverse waves propagating along the free string was determined so that the measured reflection and transmission amplitudes could be corrected.

Judging from the report the experiments were done carefully and with some expertise. Initially the researchers had expected to discover bow-resonance effects in the reflection and transmission data. This not being the case the working hypothesis seems to have been that bending stiffness is the sole agent of frequency dependence in the results.

4.2. Thick nylon string

In Figures 11(a)–(d) theoretical results are displayed and compared with the magnitudes of the transverse reflection and transmission coefficients from the experiment employing string No.1 (3 mm nylon), the experimental results Cremer published ([3] page 129).

The first graph, Figure 11(a), shows the results from Cremer's calculation (stiff string, rigid point-bow), in which he set the dimensionless string parameter $\kappa = (B/T)^{1/2}/c_0$ to $\kappa = 6 \times 10^{-5}$. This amounts to choosing the Young's modulus of the string to be $E = 35$ GPa, which is an order of magnitude greater than the values $E = 2$–4 GPa given for nylon in the literature. This experiment and the corresponding calculation were used to argue that bending stiffness is responsible for the frequency dependence of the reflection and transmission behaviour. In Figure 11(b) the prediction from the rigid finite-width model (solid lines), the first natural improvement of Cremer's model, is displayed. Figure 11(b) also features Cremer's point-bow prediction (dashed lines), but now both calculations use the value of the Young's modulus of the string $E = 4$ GPa. Clearly a rigid-bow model, be it a point-bow or a finite-width model, fails to describe the system behaviour accurately when realistic physical parameters are used.

Allowing for bow-hair elasticity (Figure 11(c)) leads to better models. The spring constant is $s = 6 \times 10^6$ (N/m)/m for the finite-width bow, the value established in Section 2 for the violin bow with $b = 10$ mm, and $S = sb$ for the point bow. The models can be further improved by taking into account bow-hair damping (Figure 11(d)). The damping constant is $d = 1000$ (kg/s)/m for the finite-width bow and $D = db$ for the point bow. The models including compliance show good agreement with the experimental data. The effect of bending stiffness is small. In fact, closer fits are achieved for values of the Young's modulus smaller than the conserva-

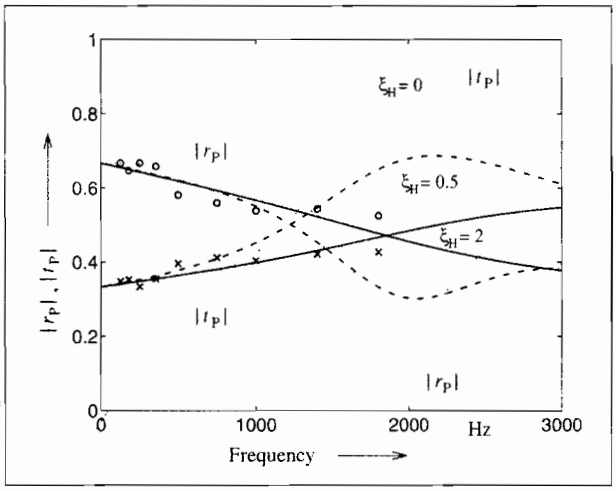

Figure 12. Transverse reflection and transmission coefficients using the "continuum" model in a finite-width calculation, compared with experimental results for Eisenberg's string No.1. A loss factor of $\xi_H \approx 2$ provides the best fit. Bow-hair modelled with $z_\infty = 790$ (kg/s)/m according to Table I.

tive estimate of $E = 4$ GPa. Values of s and d within $\pm 30\%$ of what is used throughout lead to reasonably good fits.

The differences between the point-bow and the finite-width predictions in the rigid case are large but this is due to the non-physical edge forces inherent to the assumption of a rigid support. In the two compliant cases the differences are small, hardly surprising since the shortest wavelength studied was of the order of 15 bow widths.

In all the experiments the string tension was high compared to those of strings on instruments, so the results give a slightly distorted picture. Roughly speaking, finite-width effects are wavelength dependent while compliance effects are frequency dependent. These experimental results therefore shed light on the effects of compliance rather than finite width. Bending stiffness plays a smaller role when the tension force is high so it is not surprising to find that bending stiffness plays no major role in the results given in Figure 11. However, the experiment conducted with the 3 mm steel string (Figure 13), most certainly too stiff for musical purposes, does cover the effects of bending stiffness.

Table IV summarises the frequency and wavelength range covered by the experiments.

If one imagines the strings from this experiment to be mounted at lengths corresponding to string lengths of instruments while keeping the tension the same, then one can calculate a nominal fundamental frequency, the highest nominal harmonic covered by the investigation and finally Schelleng's [25] inharmonicity measure. According to this exercise, based on the limited number of nominal harmonics covered by the measurements, strings No.1 and 3 fulfil Schelleng's criterion ($b_S < 1$) more or less, whereas the bending stiffness of the steel string No.2 is far beyond what is regarded as acceptable.

This is a convenient place to compare the two models of longitudinal bow-hair behaviour developed in Section 2, the spring-dashpot model of equation (1) which was used

Table IV. Minimum and maximum frequency ν_{min} and ν_{max} and minimum wavelength λ_{min} covered by the measurements. Imagine the experiment strings to have the length l^* of the "real" strings they are identified with in Table III. One can then deduce a fundamental frequency ν_0, the highest harmonic n_{max} covered by the investigation and the inharmonicity b_S. Note the very high frequencies, resulting from the high tensions used in the experiment.

No.	ν_{min} [Hz]	ν_{max} [Hz]	λ_{min} [cm]	l^* [m]	ν_0 [Hz]	n_{max}	b_S
1	125	1800	15.0	1.060	125	14	0.2
2	125	1800	9.0	1.060	75	24	4.4
3	125	5000	8.5	0.329	650	8	0.1

for the predictions in Figures 11(c) and (d), and the continuum model of equation (4). Figure 12 presents an example of the continuum model. Only the results from the finite-width model are shown, as again there is little difference between point and finite-width calculations. Theoretical results with increasing loss factor $\xi_H = 0$, 0.5 and 2 are given. The continuum model exhibits bow-hair resonances in the reflection and transmission behaviour, their vigour depending on the value of the loss factor. The best match is obtained with the highest loss factor, when the effects of resonance have been concealed. The theoretical results match the experimental data no better than the results obtained with the much simpler spring-dashpot model. The apparent need for implausibly high bow-hair damping to match the experimental results might perhaps be a consequence of our assumption that the bow-stick is rigid.

4.3. Steel string

The next case considered is that of the steel string interacting with the bow, seen in Figure 13.

The predictions are calculated using the spring-dashpot model and match the experimental results well. Rigid bow models would entirely fail to predict the strong changes in the reflection and transmission coefficients. In this case bending stiffness plays a significant role in the dispersive behaviour. Good fits are possible with Young's moduli for the string of $E = 100$–200 GPa, and bow parameters within $\pm 30\%$ of what is used throughout.

If a calculation of the static distribution of the bow force across the bow width (presented in Part III of this study) is performed for the strings used in the reflection and transmission experiments, one finds that the distribution of the bow force must have been close to uniform, with no more than 10% deviation from the mean value. The analysis of the distribution of the friction force indicates that it was also evenly distributed. One can therefore conclude that partial slipping was unlikely to have occurred in the reflection and transmission experiment. This finding validates the experimental evidence. If slipping were to have occurred even for parts of the period or parts of the section of string under the bow, the modelling and the interpretation of the experimental data which has just been presented would have been *a priori* flawed.

ACUSTICA · acta acustica
Vol. 84 (1998)

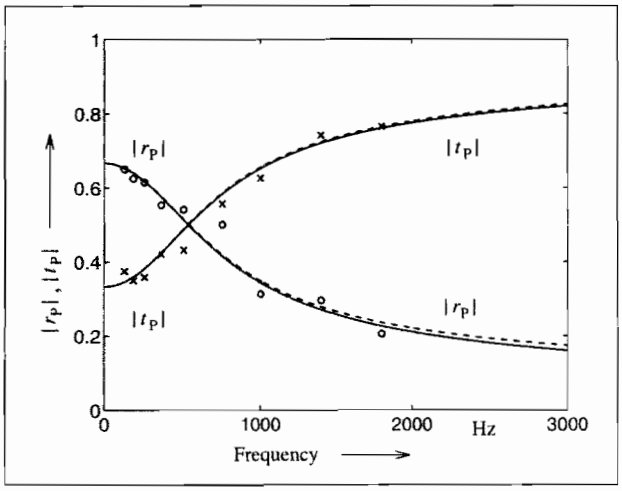

Figure 13. Transverse reflection and transmission coefficients from experimental investigation for Eisenberg's string No.2 (3 mm steel) under a violin bow, and corresponding predictions, versus frequency. String modelled with $E = 130$ GPa. Solid lines: compliant finite-width model. Dashed lines: compliant point-bow model.

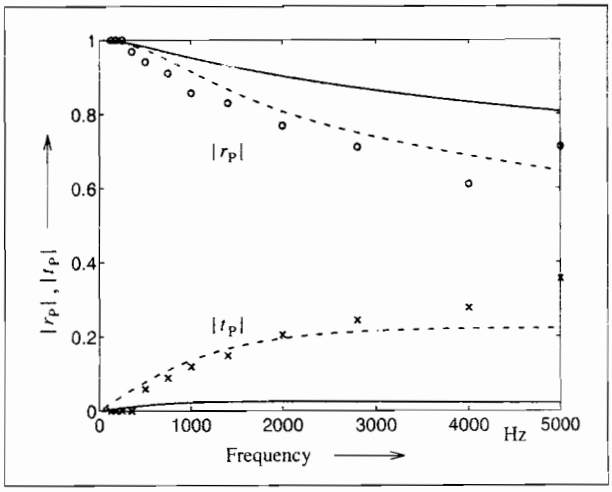

Figure 15. Transverse reflection and transmission coefficients for Eisenberg's string No.3 (1 mm nylon) on a real bow, and corresponding predictions for a string prevented from rolling, i.e. executing transverse motion only. Solid lines: finite-width model with usual compliance. Dash-dot lines: finite-width model with increased compliance $s = 2 \times 10^6$ (N/m)/m and $d = 150$ (kg/s)/m.

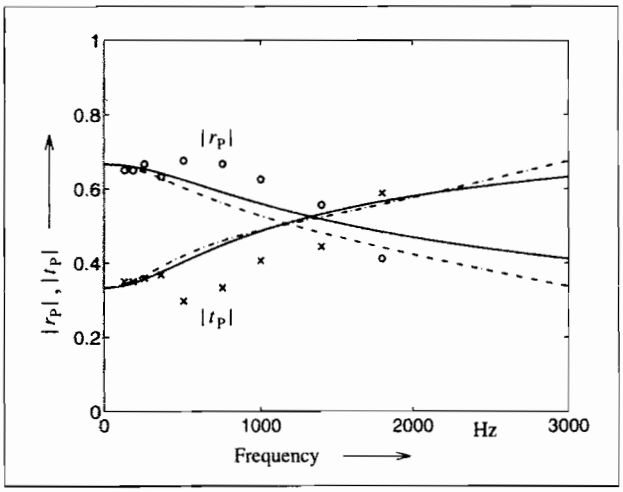

Figure 14. Transverse reflection and transmission coefficients from Eisenberg's string No.2 (3 mm steel) on a "rigid" bow with $b = 4$ mm and the corresponding predictions, versus frequency. Solid lines: compliant finite-width model with $s = 10^8$ (N/m)/m and $d = 1000$ (kg/s)/m. Dash-dot lines: rigid finite-width model. To be compared with the case using the same string and a real bow in Figure 13. Here, transmission is clearly hindered.

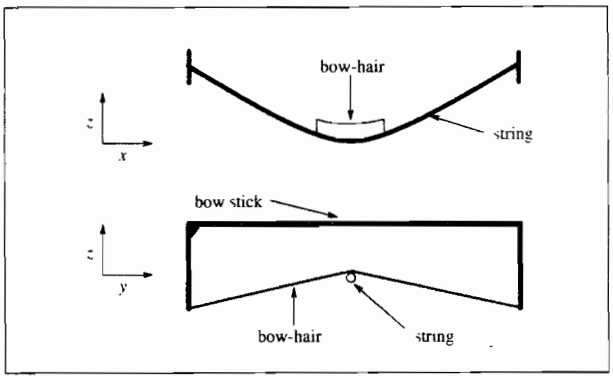

Figure 16. Schematic representation of the geometry of the contact of bow and string for high bow forces when rolling may be inhibited.

Experimental results for the reflection and transmission behaviour of a string (Eisenberg's string No.2) in contact with a "rigid" bow, a strip of nylon glued onto a strip of steel with $b = 4$ mm, are shown in Figure 14. There is some scatter in the measured reflection and transmission behaviour but one can see that the "rigid" bow is less penetrable for incident high-frequency waves than the normal, compliant bow for the same string (Figure 13). If this "bow" had been perfectly rigid some amount of slipping would have occurred. There is no evidence of slipping in the experimental results, so it seems appropriate to model the reflection and transmission behaviour using the compliant finite-width model, with a high value for the spring constant modelling the bow-hair. The exact value of the spring constant to be used for the calculation, a matter of guesswork, is not important: values $s = 10^8$ (N/m)/m and $d = 1000$ (kg/s)/m are used here. In modelling we can, however, force the string to stick to a perfectly rigid bow. The results of such a calculation are given by the dash-dot lines in Figure 14. The predictions from the perfectly rigid and the "near-rigid" model differ very little.

4.4. Thin nylon string

The next case to be discussed was dismissed by Eisenberg as erroneous but becomes meaningful when bow-hair compliance is allowed for. In Figure 15 the measured reflection and transmission behaviour for Eisenberg's string No.3 (1 mm nylon) under a real bow is displayed. Eisenberg observed that the string was deformed very significantly under the influence of the bow force. In Figure 16 the geometry of

the contact area is sketched with the displacements in the z-direction exaggerated. Strong curvature of the string (top sketch) as well as strong curvature of the ribbon of bow-hair (bottom sketch) can act to inhibit rolling motion, because the string is now in a "potential well" and would have to move "uphill" to roll. Eisenberg's observation of the string deformation is consistent with the measured reflection and transmission behaviour. For $\omega \to 0$, there is full reflection and no transmission. At higher frequencies, however, a considerable amount of transmission was measured.

A corresponding model of non-rolling interaction of a compliant bow and a string will be developed in the next section. Predictions calculated with that model are shown in Figure 15. The solid lines correspond to values of the spring and damping constants as used above. A good fit (dash-dot lines) is only achieved when the value of s is set to about one third of what has been used throughout. Reducing d to one third of the previous value for frequencies below 1000 Hz and to one sixth of the previous value for the remainder of the frequency range gives the best fit. Bending stiffness is small and plays a minor role. So far no entirely convincing explanation for the bow being seemingly more compliant in this case has been found. One reason may be that the ribbon of hair is squeezed into a narrower bundle due to the string deformation in the perpendicular plane. A reduced bow width means a more compliant bow if the thickness of the layer of bow-hair actually carrying the friction force remains the same.

5. Non-rolling contact

Two types of situations can occur in which bow and string interact without rolling motion. First, and more obvious, on a bowed string there are waves propagating on the string in the *perpendicular plane*, which are either generated when waves in the bowing plane impinge on the bridge [26, 27], by nonlinear coupling of the motion in the two planes, or excited through bow motion in the perpendicular plane itself. Waves in the perpendicular plane interact with the bow and lead to perturbations of the bow force which may significantly alter the temporal and spatial distribution of slipping and sticking under the bow. Secondly, as was observed by Eisenberg, strong static deformation of the string and bow may lead to inhibition of rolling motion of a string moving in the bowing plane: transverse motion remains, torsional motion subsides.

The mathematical treatment of the contact problem for these two situations is identical, the difference lying only in the impedance presented to the string by the bow. The equations describing these situations will be derived and discussed in terms of the string motion in the bowing plane. The discussion of the perpendicular plane is deferred to Part III of this study.

The point-bow model of the reflection and transmission behaviour for the non-rolling case can either be inferred from equation (23) by letting the torsional impedance $Z_T \to \infty$, or by doing the calculation from first principles. The resulting formulae for the reflection coefficient and the friction force are:

$$r_P = \frac{-1}{\left(1 + \frac{2Z_S}{Z_H}\right)\left(1 + \frac{k_P}{k_E}\right)}, \qquad F = \frac{-i\omega 2Z_S}{1 + \frac{2Z_S}{Z_H}}. \tag{44}$$

As in the rolling case, the transmission coefficient is $t_P = 1 + r_P$ and the near-field amplitudes are $r_E = t_E = (k_P/k_E)\, r_P$. The impedance Z_H represents the longitudinal behaviour of the bow at the bowing point as before.

The finite-width case is modelled as follows: if there is no angular displacement of the string, the motion of such a string under the bow is described by the equation of momentum (25) only. The displacement η_H of the bow-hair and displacement η of the string on the line of contact are then identical. Elimination of the friction force in the equation of momentum (25) using the constitutive relation results in:

$$T \frac{\partial^2 \eta}{\partial x^2} - B \frac{\partial^4 \eta}{\partial x^4} - z_H \frac{\partial \eta}{\partial t} = m \frac{\partial^2 \eta}{\partial t^2}. \tag{45}$$

With $z_H = -is/\omega + d$ and assuming time-harmonic motion, the corresponding dispersion relation is then

$$\left(\omega^2 - c_0^2 k^2 - \frac{B}{m} k^4\right) - \frac{1}{m} i\omega z_H = 0 \tag{46}$$

from which one can compute two wavenumbers. For the purpose of a clearer explanation the undamped system is studied first. At low frequencies both wavenumbers are imaginary and correspond to evanescent waves. One of the wavenumbers turns real for higher frequencies. The cut-on frequency is $\omega_c = (s/m)^{1/2}$, the resonance frequency for the continuum of the distributed mass (the string) and the distributed spring (the bow-hair). Damping "blurs" the cut-on behaviour somewhat. For the string of the example given in Figure 15, the theoretical cut-on frequency is 7600 Hz, beyond the frequency range covered by the experiment.

For the solution of the reflection and transmission problem the four jump conditions pertaining to the transverse motion have to be satisfied at each interface. As an ansatz for the waves on the *free* string only those parts of the wave ansatz equations (11) pertaining to the transverse motion are used. Under the bow ($0 \le x \le b$) the ansatz is

$$\eta = \left(t_1 e^{-ik_1 x} + t_2 e^{-ik_2 x}\right) e^{i\omega t} + \left(r_1 e^{ik_1 x} + r_2 e^{ik_2 x}\right) e^{i\omega t}, \tag{47}$$

where k_1 and k_2 are the solutions to equation (46). Examples of the results of such calculations are given in Figure 17 for the point-bow and the finite-width model. The inharmonicity parameter is set to $b_S = 0.1$ throughout and the bow parameters are set as usual. In the undamped case, not shown here, transmission is higher for the finite-width bow than for the point bow; this is due to the jump in impedance from the free string to the string under the bow being smaller in the finite-width case. In the damped case, Figure 17, we note that the finite-width bow is more efficient at dissipating energy.

ACUSTICA acta acustica
Vol. 84 (1998)

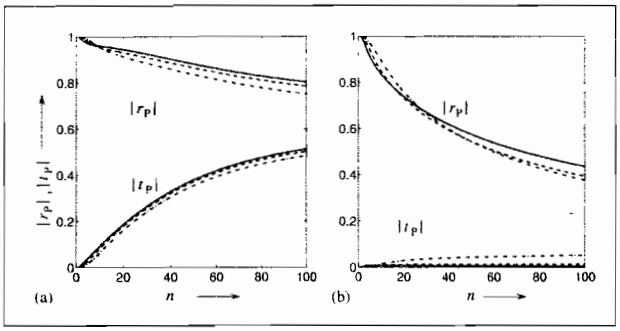

Figure 17. Non-rolling reflection and transmission of waves. Reflection and transmission coefficients versus harmonic number n for (a) point-bow and (b) finite-width model. Strings 1–4 from Table II, represented by different line-types as in Figures 5 and 10. Bow parameters as usual (Table I).

To shed some light on this particular reflection and transmission behaviour of the string under the finite-width bow one may look again at the wavenumbers arising from the dispersion relation. At low frequencies when both wavenumbers correspond to non-propagating waves there is little transmission. The fact that even though the string is prevented from rolling, there is an increase of the transmission coefficient with frequency can be seen as due to a tunnelling mechanism: the near-field of the cut-on wave reaches through the bow into the section of free string on the other side of the bow and transmits energy. With increase in frequency, both the range and the amplitude of the near-fields of the cut-on wave grow, and more and more energy is transmitted. Above the cut-on frequency transmission takes place via the propagating cut-on wave.

Only a model of the bow allowing for bow-hair compliance can give a satisfactory explanation for the case given in Figure 15. It would be worthwhile investigating the extent to which the case of the string being prevented from rolling occurs in actual bowed-string motion; but this issue must be deferred to another occasion.

6. Discussion

The analysis presented here of the behaviour of a string in contact with a bow *at rest* is valid for a *bowed* string during the sticking episode of the Helmholtz cycle in a reference frame moving with the velocity of the bow. It may be recalled that in idealised Helmholtz motion the string at the bowing point moves with the velocity of the bow during sticking. In any more realistic form of Helmholtz motion the perturbations superimposed on the waveform of the idealised Helmholtz motion (including torsional motion) will interact with the bow in the way set out here while the string is sticking to the bow.

A good model of the *bowed* string should take into account as many physical details as possible, certainly including finite bow width. All models currently in use are, however, point-bow models or extended point-bow models. These models usually assume a perfectly flexible string in the vicinity of the bow. Implementing finite bow width or bending stiffness into simulation programs of the bowed string is cumbersome. The efficiency of the simulation schemes using the "rounded-corner model" with its point-bow approximation is lost. Implementing bow-hair compliance on its own is a relatively easy task. A useful question to ask is: which level of sophistication between that of the simple, conventional model and that of an involved model comprising finite width, bow-hair compliance and bending stiffness is adequate? What is the tradeoff between physicality and economy? The answer may depend on the particular purpose of the investigation and on the combination of bow, string and instrument studied. On the basis of the present analysis and the available experimental evidence we can attempt to answer this question by considering the reflection and transmission behaviour of the family of models presented so far. Which model is suitable for the description of phenomena present during *slipping* will be the issue of Parts II and III.

With so many parameters to vary it is difficult to make very general statements about the characteristics and the suitability of the various models. The strings of instruments of the violin family differ enormously with respect to the transverse impedance ($Z_0 = 0.2$–5.5 kg/s), the ratio of torsional to transverse impedance ($Z_T/Z_0 = 1$–5) and the bending stiffness. Schelleng's measure of inharmonicity b_S can vary between as little as 0.04 for a steel violin E string and as much as 2.3 for a gut violin G string [25].

One attempt to assess the importance of the various possible ingredients of a more involved model of the bowed string consists of analysing how the predictions calculated on the basis of different models compare with Eisenberg's experimental results. In all the cases investigated, bow-hair elasticity is crucial to the explanation of the reflection and transmission behaviour. Damping is an important feature in all cases, although a fairly good fit can be achieved with a broad range of damping values. Bending stiffness is important in the case of the steel string but plays virtually no role in the case of the two nylon strings. Width-related effects are not covered by the experimental work as the smallest wavelengths investigated were an order of magnitude larger than the bow width.

For a more complete overview one can make use of the results presented in Figures 5 and 10. Both perfectly flexible strings and stiff strings were considered. The dimensions of the model bows were adjusted to the particular instruments.

To summarise some general observations for point-bow models: for the model of the stiff string on the rigid point-bow the reflection and transmission curves for all strings with the same amount of inharmonicity collapse. Bow-hair elasticity brings out differences in behaviour between strings. It affects the reflection and transmission behaviour of strings more when Z_T/Z_0 is high. The effects of bow-hair compliance are smaller if the bending stiffness of the string is high. For the higher strings (with low transverse impedance) the damped bow resembles a rigid bow. Energy dissipation is highest for the lower strings.

Now for finite-width models: for an important part of the relevant frequency range the rigid finite-width bow is less permeable for transverse waves on a stiff string than the

conventional model. The transmission of transverse waves increases for all strings when bow-hair elasticity is taken into account. The amount of energy converted into torsional motion is greater than for point-bow models. Finite-width models predict substantially higher losses than point-bow models; these are again highest for the lower strings. For all strings the effect of bending stiffness, if Schelleng's suggested limit is respected, is very small. For strings with the same impedance ratio the scaling of the bows (width and length of hair) for the different instruments of the violin family works towards collapsing the reflection and transmission curves of the corresponding strings. Bow-hair damping has a similar effect.

What can now be said concerning the suitability of models? The point-bow model based on a perfectly flexible string and undamped but elastic bow hair is an improvement compared with the conventional model. However, damping at the level estimated in Section 2 turns the point-bow into an unrealistically rigid bow for low impedance strings. Bending stiffness, if included, has a stronger effect than finite-width calculations lead us to believe is realistic.

The rigid point-bow model paired with bending stiffness may be acceptable for rather stiff strings ($b_S = 1$), and especially for strings with low transverse impedance, in cases in which bow-hair damping is thought to be unimportant. If one applies a rigid bow model in cases where it is inappropriate to do so, one potentially computes perturbations of the friction force resulting from perturbations in the displacement or velocity waveform which are unrealistically high. In effect one is setting Z_0/Z_H in equation (23) to zero. If one keeps to realistic values of the (normal) bow force, the perturbations of the friction force may exceed limiting friction. This analysis suggests one reason why, when bowing a string with a rigid rod, it is difficult to produce regular Helmholtz motion.

Rigid finite-width models lead to non-physical results, namely the singular edge forces. Bending stiffness renders the bow even less permeable for an important part of the relevant frequency range. In compliant finite-width models bending stiffness corresponding to Schelleng's suggested limit of inharmonicity has only a small effect on the reflection and transmission behaviour whereas bow-hair compliance has a strong influence. Damping can affect predictions of point-bow and finite-width models quite differently.

To summarise, from the present point of view it seems advisable when moving away from the conventional model of the perfectly flexible string paired with the rigid point-bow to take into account bow-hair compliance first. Allowing for the finite width is essential for the modelling of differential motion in the context of the *bowed* string. With respect to the reflection and transmission problem, bending stiffness seems to be more important to include in the artificial point-bow models than in the more realistic finite-width models where the dispersive behaviour is hardly altered for inharmonicity levels of $b_S \leq 0.1$. This suggests that priority should be given to including the finite width over modelling the bending stiffness in the vicinity of the bow.

Torsional motion is normally present in actual bowed strings. Whether, however, situations occur in actual bowing in which rolling motion is inhibited as in the case of shown in Figure 15 remains speculation. A model of a non-rolling string on a compliant bow has been given in Section 5, and it seems to explain the important features of Eisenberg's experimental results. Mixed models in which rolling motion is still possible but hindered could also be constructed.

Both the damped point-bow and the damped finite-width model predict an increase in dissipation with increase in the impedance ratio Z_T/Z_0. The prime reason for this is that less energy is converted into the rolling motion which would take place with a smaller friction force and therefore less bow-hair deformation. This is an interesting result: for low values of Z_T/Z_0 a large fraction of the incident wave energy is converted into torsional energy, but is then subject to the relatively high rate of torsional damping on the free string. For high values of Z_T/Z_0 little energy is converted but a larger fraction is dissipated through bow-hair damping. This might be a reason why such a large range in impedance ratio is acceptable for bowed strings.

As a final comment in this section, recall Friedlander's [6] suggestion that the width of the bow might affect the string motion in a similar way to a mass of size $M = mb$ at the bowing point. This idea can be elucidated by altering the point-bow models described in Section 3.1 to include additional inertia terms in the jump conditions. The effect of the added mass is small. The added inertia terms model a blocking mass in a transmission line, which increases the reflection coefficient and decreases the transmission coefficient. Friedlander's approximation is qualitatively correct in the context of the unrealistic rigid-bow models, but it is an inadequate description in more realistic models taking into account bow-hair compliance. When Friedlander's suggestion is incorporated into the compliant bow model it predicts effects which sometimes have the wrong sign. It does not seem to be a fruitful suggestion to follow in bowing models.

7. Conclusions

A physical model of the contact area between bow and string has been developed which takes into account the width of the bow, the bending stiffness of the string, the longitudinal bow-hair compliance and the torsional motion of the string. Despite being mathematically simple it is capable of capturing details for which there is existing experimental evidence but hitherto no satisfactory explanation. This evidence comes from an experiment carried out by Cremer [3], Eisenberg and Lazarus [4] in which the reflection and transmission behaviour of waves travelling on a long string in contact with a stationary bow was studied. As well as giving insight into the details of the reflection and transmission behaviour of a string rolling on the surface of the bow-hair this model is also suitable for the implementation in numerical simulations of the bowed string, as will be shown in two companion papers [1, 2].

The comparison of analytical and experimental results demonstrates that models which neglect bow-hair compliance give wrong predictions of the reflection and transmis-

ACUSTICA · acta acustica
Vol. 84 (1998)

sion behaviour for a real bow. The modelling of bow-hair compliance is important for two reasons. Firstly, it improves the quantitative predictions computed using *point-bow* models. Secondly, only if bow-hair compliance is taken into account do *finite-width* models give a worthwhile improvement over the much simpler point-bow models. This is due to the fact that the assumption of rigid bow-hair leads to singular forces at both edges of the bow which are removed when bow-hair compliance is allowed for. The analysis presented here suggests that finite-width effects may be significant during the sticking episode of the Helmholtz cycle. Combined effects of bow width, bow-hair elasticity, bow-hair damping and bending stiffness create a wide range of different regimes. On the whole, bending stiffness has been shown to play only a rather minor role in the reflection and transmission behaviour as long as Schelleng's [25] suggested inharmonicity threshold is roughly respected. Point-bow models are misleading in that they suggest that bending stiffness plays a bigger part in transmission of wave energy than it actually can on a realistic, finite-width bow.

References

[1] R. Pitteroff, J. Woodhouse: Mechanics of the contact area between bow and string. Part II: Simulating the bowed string. Acustica - acta acustica (1998). to be published.

[2] R. Pitteroff, J. Woodhouse: Mechanics of the contact area between bow and string. Part III: Parameter dependence. Acustica - acta acustica (1998). to be published.

[3] L. Cremer: The physics of the violin. MIT Press, Cambridge, MA, USA, 1985.

[4] P. Eisenberg: Reflexionsfaktor des Geigenbogens. 1968. Project report, ITA, TU Berlin.

[5] C. V. Raman: On the mechanical theory of bowed strings and of musical instruments of the violin family, with experimental verification of results: Part I. Bull. Indian Ass. Cult. Sci. **15** (1915) 1–158.

[6] F. G. Friedlander: On the oscillations of a bowed string. Proc. Cam. Phil. Soc. **49** (1953) 516–530.

[7] M. E. McIntyre, R. T. Schumacher, J. Woodhouse: Aperiodicity in bowed-string motion. Acustica **49** (1981) 13–32. See also next reference.

[8] M. E. McIntyre, R. T. Schumacher, J. Woodhouse: Aperiodicity in bowed-string motion: On the differential-slipping mechanism. Acustica **50** (1982) 294–295.

[9] J. Woodhouse: On the playability of violins. Part II: Minimum bow force and transients. Acustica **78** (1993) 137–153.

[10] X. Boutillon: Analytical investigation of the flattening effect: The reactive power balancing rule. J. Acoust. Soc. Am. **90** (1991) 754–763.

[11] R. T. Schumacher: Some aspects of the bow. Catgut Acoust. Soc. Newsletter **24** (1975) 5–8.

[12] J. M. Adrien, E. Ducasse: Dynamic modeling of instruments for sound synthesis. Proceedings 13th ICA Belgrad, Yugoslavia, 1989. 105–108.

[13] K. Guettler: The bowed string computer simulated — some characteristic features of the attack. Catgut Acoust. Soc. Journal **2** (1992) 22–26.

[14] F. S. Gillan, S. J. Elliot: Measurements of the torsional modes of vibration of strings on instruments of the violin family. Journal of Sound and Vibration **130** (1989) 347–351.

[15] R. E. Menzel, R. Marcus: The microstructure of horse hair. Catgut Acoust. Soc. Newsletter **32** (1979) 14–20.

[16] F. Rocaboy: The structure of bow-hair fibres. Catgut Acoust. Soc. Journal **1** (1990) 34–36.

[17] A. Askenfelt: Observations on the violin bow and the interaction with the string. Speech Transmission Quarterly Progress and Status Report, Royal Institute of Technology, Stockholm **2–3** (1995) 23–41.

[18] R. T. Schumacher: (personal communication). 1994.

[19] N. Fletcher, T. Rossing: The physics of musical instruments. Springer, New York, 1981.

[20] G. Weinreich, R. Caussé: Elementary stability considerations for bowed-string motion. J. Acoust. Soc. Am. **89** (1991) 887–895.

[21] G. Dick: Metten, Germany. (catalogue). 1994.

[22] N. C. Pickering: Physical properties of violin strings. Catgut Acoust. Soc. Newsletter **44** (Nov. 1985) 6–8.

[23] C. W. Field: A study of the effect of string characteristics on the performance of the alto violin. Catgut Acoust. Soc. Newsletter **42** (Nov. 1984) 22–25.

[24] SAVAREZ/SOVAC: String manufacturer, Suze La Rousse, France. (personal communication). 1994.

[25] J. C. Schelleng: The bowed string and the player. J. Acoust. Soc. Am. **53** (1973) 26–41.

[26] C. Gough: The theory of string resonances on musical instruments. Acustica **49** (1981) 124–141.

[27] X. Boutillon, G. Weinreich: Measurement of the three-dimensional admittance at a violin bridge. Proceedings 13th ICA Belgrad, Yugoslavia, 1989. 87–90.